The Response of the Amazon Ecosystem to the Photosynthetically Active Radiation Fields: Integrating Impacts of Biomass Burning Aerosol and Clouds in the NASA GEOS Earth System Model

Huisheng Bian[1,2], Eunjee Lee[3,4], Randal D. Koster[4], Donifan Barahona[4], Mian Chin[2], Peter R. Colarco[2], Anton Darmenov[2], Sarith Mahanama[5,4], Michael Manyin[5,4], Peter Norris[3,4], John Shilling[6], Hongbin Yu[2], and Fanwei Zeng[5,4]

[1]Joint Center for Environmental Technology UMBC, Baltimore, MD, 21250, USA
[2]Laboratory for Atmospheres, NASA Goddard Space Flight Center, Greenbelt, MD, 20771, USA
[3]Goddard Earth Sciences Technology and Research, Universities Space Research Association, Columbia, MD 21046, USA
[4]Global Modeling and Assimilation Office, NASA Goddard Space Flight Center, Greenbelt, MD 20771, USA
[5]Science Systems and Applications, Inc., Lanham, MD 20706, USA
[6]Atmospheric Sciences & Global Change Division, Pacific Northwest National Laboratory, Richland, WA 99352, USA

Correspondence to: Huisheng Bian (Huisheng.Bian@nasa.gov)

Abstract

The Amazon experiences fires every year, and the resulting biomass burning aerosols, together with cloud particles, influence the penetration of sunlight through the atmosphere, increasing the ratio of diffuse to direct photosynthetically active radiation (PAR) reaching the vegetation canopy and thereby potentially increasing ecosystem productivity. In this study, we use the NASA Goddard Earth Observing System (GEOS) model with coupled aerosol, cloud, radiation, and ecosystem modules to investigate the impact of Amazon biomass burning aerosols on ecosystem productivity, as well as the role of the Amazon's clouds in tempering this impact. The study focuses on a seven-year period (2010-2016) during which the Amazon experienced a variety of dynamic environments (e.g., La Niña, normal years, and El Niño). The direct radiative impact of biomass burning aerosols on ecosystem productivity—called here the aerosol diffuse radiation fertilization effect —is found to increase Amazonian Gross Primary Production (GPP) by 2.6% via a 3.8% increase in diffuse PAR (DFPAR) despite a 5.4% decrease in direct PAR (DRPAR) on multiyear average during burning seasons. On a monthly basis, this increase in GPP can be as large as 9.9% (occurring in August 2010). Consequently, the net primary production (NPP) in Amazon is increased by 1.5%, or ~92 TgCyr^{-1}– equivalent to ~37% of the average carbon lost due to Amazon fires over the seven years considered. Clouds, however, strongly regulate the effectiveness of the aerosol diffuse radiation fertilization effect. The efficiency of this fertilization effect is the highest in cloud-free conditions and linearly decreases with increasing cloud amount until the cloud fraction reaches ~0.8, at which point the aerosol-influenced light changes from being a stimulator to an inhibitor of plant growth. Nevertheless, interannual changes in the overall strength of the aerosol diffuse radiation fertilization effect are primarily controlled by the large interannual changes in biomass burning aerosols rather than by changes in cloudiness during the studied period.

47
1. Introduction

48
49
The Amazon is home to more than 34 million people and hosts a large variety of plants and
50
animals. The rainforest plays a vital role in the global climate, regulating temperatures and
51
storing vast quantities of carbon (Laurance 1999; Nepstad et al., 2008). It is matter of intense
52
research whether light or water is the limiting factor that controls plant growth over Amazonia.
53
Considerable evidence demonstrates that sunlight indeed drives Amazon forest growth (Doughty
54
et al., 2019; Huete et al., 2006; Myneni et al., 2007) although water deficit could be a limiting
55
factor during severe droughts (Doughty et al., 2015; Feldpausch et al., 2016; Saatchi et al.,
56
2013). Satellite observations show a clear seasonal cycle with a gradual crescendo in both leaf
57
area and incoming surface sunlight beginning at the onset of the dry season (~August –
58
November) (Myneni et al., 2007). Vegetation index maps also show that a majority of Amazonia
59
is greener in the dry season than in the wet season (~mid-December – mid-May) (Huete et al.,
60
2006). It is in the dry season, when more light reaches the canopy level, that the Amazon forest
61
thrives.

62
63
Plant photosynthesis requires sunlight to reach the leaves of the canopy. While aerosols and
64
clouds in the atmosphere decrease the total amount of light that reaches the canopy, they also
65
increase scattering, thereby increasing the ratio of diffuse radiation to direct radiation. This is
66
important because the efficiency of plant photosynthesis increases under diffuse sunlight – a
67
phenomenon both explained theoretically (Rap et al., 2015; Roderick et al., 2001; Zhou et al.,
68
2020) and observed in the field (Cirino et al., 2014; Doughty et al., 2010; Ezhova et al., 2018; Gu
69
et al., 2003; Lee et al., 2018; Niyogi et al., 2004; Oliveira et al., 2007). Leaf photosynthesis
70
increases nonlinearly with solar radiation, becoming saturated on bright days at light levels
71
above which leaves cannot take more light (Gu et al., 2003; Mercado et al., 2009). Under clear
72
and clean sky conditions, particularly around midday, sunlight is mainly direct, and while this
73
allows the sunlit leaves on top to be light saturated, the shaded leaves below them receive
74
relatively little sunlight and thus participate less in photosynthesis (Rap et al., 2015; Roderick et
75
al., 2001). In contrast, under cloudy conditions or in the presence of aerosols, much of the
76
midday light is diffuse, and diffuse light can penetrate deeper into the canopy and illuminate
77
shaded leaves. Li and Yang (2015) conducted a chamber experiment to explore diffuse light on
78
light distribution within a canopy and the resulting effects on crop photosynthesis and plant
79
growth. They concluded that diffusion of the incident light improves spatial light distribution,
80
lessens the variation of temporal light distribution in the canopy, and allows more light-
81
stimulated growth of shade-tolerant potted plants.

82
83
The situation is more profound during the Amazon dry season when intensive seasonal fires
84
release large amounts of primary aerosol particles as well as gas precursors that form secondary
85
organic and inorganic aerosols. Using stand-alone radiation and vegetation models, Rap et al.
86
(2015) concluded that fires over the Amazon dry season increase Amazon net primary
87
production (NPP) by 1.4–2.8% by increasing diffuse radiation. This enhancement of Amazon
88
basin NPP (78–156 Tg C a^{-1}) is equivalent to 33–65% of the annual regional carbon emissions
89
from biomass burning and accounts for 8–16% of the observed carbon sink across mature
90
Amazonian forests. Moreira et al. (2017) advanced this analysis by coupling an ecosystem
91
module and aerosol model within a Eulerian transport model. Their study indicated that biomass
92
burning aerosols lead to increases of about 27% in Amazonian Gross Primary Production (GPP)

93   and 10% in plant respiration as well as a decline in soil respiration of 3 %. However, their
94   approach assumes cloud-free conditions through their use of a diffuse irradiance
95   parameterization based on the multiwavelength aerosol optical depth (AOD) measurement.
96   Malavelle et al. (2019) explored the overall net impact of biomass burning aerosol on the
97   Amazon ecosystem using an Earth System Model (ESM) (HadGEM2-ES). They estimated NPP
98   to increase by +80 to +105 TgC yr^{-1}, or 1.9% to 2.7%, ascribing this net change to an increase in
99   diffuse light, a reduction in the total amount of radiation, and feedback from climate adjustments
100   in response to the aerosol forcing. Their study takes into account the dynamic feedback of short
101   lifetime cloud fields. However, the authors have not explicitly quantified the impact of Amazon
102   background clouds and their interannual changes in tempering the aerosol diffuse radiation
103   fertilization effect (DRFE).
104
105   When clouds and aerosol co-exist, the impact from clouds on the ecosystem typically dominates
106   because clouds are optically thicker. The surface sunlight for cloudy versus cloud-free conditions
107   can differ greatly even if the AOD is the same. (Note that, unless specified otherwise, solar
108   radiation in this study refers to the wavelength range of 400-700 nm, i.e., photosynthetically
109   active radiation, or PAR). Measurements indicate that the desirable range of clearness index (CI)
110   -- the ratio of total (i.e., direct plus diffuse) light at surface to the total incoming light at top of
111   atmosphere -- is around 0.4-0.7 for some forest ecosystems and above 0.3 for peatland (Butt et
112   al., 2010, Letts and Lafleur, 2005). Quite often a low CI occurs during a cloudy day, but on
113   occasion it might result from the presence of a very thick aerosol layer. As suggested above, if
114   CI is high, the diffuse fraction of the total solar radiation is low, and the overall productivity of
115   the canopy is reduced. For example, Cirino et al. (2014) found that the net ecosystem exchange
116   (NEE) of CO_2 is increased by 29% and 20% in two Amazon stations, the Jaru Biological Reserve
117   (RBJ) and the Cuieiras Biological Reserve at the K34 Large-Scale Biosphere-Atmosphere
118   Experiment in Amazonia (LBA) tower, respectively, when AOD is 0.1-1.5 at 550nm under clear
119   conditions. Higher AOD (> 3) leads to a strong reduction in photosynthesis (via reducing PAR)
120   up to the point where NEE approaches zero. Oliveira et al. (2007) found that Amazon forest
121   productivity was enhanced under moderately thick smoke loading because of an increase of
122   diffuse solar radiation, but large aerosol loading (i.e., AOD > 2.7) results in lower net
123   productivity of the Amazon forest.
124
125   Despite its name, the Amazon's "dry season" (June-November) still features significant
126   cloudiness, and the interannual variations in the clouds can be large. Furthermore, rain does fall
127   during the dry season – close to 40% of the total annual precipitation falls therein (Li et al.,
128   2006). Clouds in the dry season are mostly formed by small-scale processes that influence the
129   weather (see an example of a uniform layer of "popcorn" clouds observed by Moderate
130   Resolution Imaging Spectroradiometer (MODIS) on 08/19/2009 in
131   http://earthobservatory.nasa.gov/IOTD/view.php?id=39936). It is during this period, when
132   sunlight (particularly diffuse light) shines on the trees due to reduced rain (and fewer clouds)
133   relative to the wet season, that the forest grows the most. Consideration of the joint effects of
134   clouds and biomass burning aerosols on diffuse and direct PAR during the dry season is thus
135   particularly important.
136
137   This study has two objectives. First, we investigate how Amazon biomass burning aerosols
138   (BBaer) affect the land productivity (i.e., GPP and NPP) via their impact on direct and diffuse

139   PAR (DRPAR and DFPAR). Second, we investigate the sensitivity of the BBaer DRFE to the
140   presence of the Amazon dry season cloud fields within the range indicated by the interannual
141   variation of the clouds. We use in our analysis a version of the NASA GEOS ESM that includes
142   coupling between aerosol, cloud, radiation, and ecosystem processes. To our knowledge, only
143   one other study has used an ESM to investigate such fire impacts across Amazonia (Malavelle et
144   al., 2019), and as noted above, that study did not address the ability of Amazon clouds to temper
145   the BBaer impacts. Accordingly, our study is the first ESM-based study to investigate the BBaer
146   DRFE within a range of interannual Amazon cloud levels. Together our objectives provide a full
147   and comprehensive study of BBaer DRFE in a context of potential Amazon dry season
148   atmospheric conditions.
149
150   It is necessary to point out, however, that our study focuses only on the impact of Amazon
151   biomass burning aerosol. We do not consider the radiative impacts of other potentially important
152   aerosols. These other aerosol types have been examined in various observational studies (e.g.,
153   Cirino et al., 2014; Ezhova et al., 2018; Hemes et al., 2020; Wang et al., 2018, Yan et al., 2014)
154   and model investigations that focus, for example, on anthropogenic aerosol (Keppel et al., 2016);
155   O'Sullivan et al., 2016), dust (Xi et al., 2012), biogenic aerosol (Rap et al., 2018; Sporre et al.,
156   2019), volcanic aerosol (Gu et al., 2003), and the general aerosol field (Feng et al., 2019).
157
158   The paper is organized as follows. Section 2 describes the NASA GEOS ESM and its relevant
159   modules (section 2.1), the observational data used for model evaluation and explanation (section
160   2.2), and the experimental setup (section 2.3). Section 3 provides an evaluation of the model
161   (section 3.1), basic theory regarding the impact of aerosol and cloud on the surface downward
162   radiation (section 3.2), results regarding the simulated ecosystem response to BBaer-induced
163   radiation changes (section 3.3), and the impacts of Amazon background clouds on this response
164   (section 3.4). A final summary is provided in section 4.
165
166   **2. Model description, data application, and experiment setup**
167
168   **2.1 Model description**
169   The GEOS modeling system connects state-of-the-art models of the various components of the
170   Earth's climate system together using the Earth System Modeling Framework (ESMF) (Molod et
171   al., 2015; 2012; Rienecker et al., 2011; https://gmao.gsfc.nasa.gov/). We discuss here the
172   components of the system that are particularly relevant to our study, including aerosol, cloud
173   microphysics, radiative transfer, and land ecosystem modules.
174
175   GEOS Goddard Chemistry Aerosol Radiation and Transport (GOCART) simulates a number of
176   major atmospheric aerosol species and precursor gases from natural and anthropogenic sources,
177   including sulfate, nitrate, ammonium, black carbon (BC), organic aerosol (OA, including
178   primary and secondary OA), dust, sea salt, dimethyl sulfide (DMS), SO_2, and NH_3 (Bian et al.,
179   2010, 2013, 2017, 2019; Chin et al., 2009, 2014; Colarco et al., 2010, 2017; Murphy et al., 2019;
180   Randles et al., 2013). Monthly emissions from shipping, aircraft, and other anthropogenic
181   sources are obtained from the recent CMIP6 CEDS emission inventory. Daily biomass burning
182   emissions are provided by GFED4s
183   (https://daac.ornl.gov/VEGETATION/guides/fire_emissions_v4.html). Estimates of degassing
184   and eruptive volcanic emissions are derived from Ozone Monitoring Instrument (OMI) satellite

185   (Carn et al., 2017). Emissions of dust, sea salt, and DMS are dynamically calculated online as a
186   function of the model-simulated near-surface winds and other surface properties. A more recent
187   development of GOCART relevant to this study involves the modification of the absorbing
188   properties of "brown carbon" from biomass burning organic aerosols (Colarco et al., 2017) and
189   the inclusion of secondary organic aerosol (SOA) produced via chemical reactions of volatile
190   organic compounds (VOCs) emitted from anthropogenic and biomass burning sources, following
191   the approach developed by Hodzic and Jimenez (2011) and Kim et al. (2015). In addition, the
192   SOA from biogenic sources has been updated with its precursor gases of isoprene and
193   monoterpene emissions calculated online as a function of light and temperature using the Model
194   of Emissions of Gases and Aerosols from Nature (MEGAN) version 2.1 (Guenther et al., 2012),
195   assuming SOA yield of 3% from isoprene and 5% from monoterpene oxidations (Kim et al.,
196   2015).
197
198   The GEOS two-moment cloud microphysics module is used in this study. The module includes
199   the implementation of a comprehensive stratiform microphysics module, a new cloud coverage
200   scheme that allows ice supersaturation, and a new microphysics module embedded within the
201   moist convection parameterization (Barahona et al., 2014). At present, aerosol number
202   concentrations are derived from the GEOS/GOCART-calculated aerosol mass mixing ratio and
203   prescribed size distributions and mixing state, which are then used for cloud condensation nuclei
204   (CCN) activation (following the approach of Abdul-Razzak and Ghan, 2000) and ice nucleation
205   (following the approach of Barahona and Nenes, 2009) processes. Aerosol-cloud interactions are
206   thus accounted for in our simulation. The model calculates various cloud properties, including
207   cloud fraction, cloud droplet and ice crystal number concentrations and effective radii, and cloud
208   liquid and ice water paths. These fields have been evaluated against satellite observations and
209   field measurements; the model shows a realistic simulation of cloud characteristics despite a few
210   remaining deficiencies (Barahona et al., 2014, Breen et al., 2020).
211
212   The current default GEOS solar radiation transfer module is the shortwave rapid radiation
213   transfer model for GCMs (RRTMG_SW), a correlated k-distribution model (Iacono et al., 2008).
214   This GCM version utilizes a reduced complement of 112 g-points, which is half of the 224 g-
215   points used in the standard RRTMG_SW, and a two-stream method for radiative transfer. Total
216   fluxes are accurate to within 1-2 W/m^2 relative to the standard RRTMG_SW (using DISORT)
217   with aerosols in clear sky and within 6 W/m^2 in overcast sky. RRTMG_SW with DISORT is
218   itself accurate to within 2 W/m^2 of the data-validated multiple scattering model, CHARTS.
219   RRTMG_SW specifically calculates the direct and diffuse components of PAR (400-700 nm)
220   separately. The GEOS atmospheric radiative transfer calculation is designed in a way that allows
221   users to examine the impact of various combinations of atmospheric aerosol and cloud fields on
222   radiation. In addition to the standard calculation of solar radiation for ambient atmospheric
223   conditions, diagnostic calculations can be carried out by repeating the calculation of the radiation
224   transfer scheme with different combinations of atmospheric conditions: clean air (no aerosols),
225   clear air (no clouds), and clean plus clear air. Using this architecture, for this study we modify
226   the radiation scheme to allow the additional diagnosis of radiation fields under conditions of zero
227   BBaer but retained non-BBaer and ambient clouds.
228
229   The catchment land surface model (LSM) with carbon and nitrogen physics (Catchment-CN) in
230   GEOS is in essence a merger of the C-N physics within the NCAR–DOE Community Land

Model (CLM) (Oleson et al. 2010, 2013; Lawrence et al., 2019) version 4.0 and the energy and water balance calculations of the NASA GMAO catchment LSM (Koster et al. 2000). The original NASA catchment LSM used a prescribed representation of phenology (leaf area index, or LAI, and greenness fraction) to compute the canopy conductance, the parameter describing the ease with which the plants transpire water. The light interception by vegetation in the GEOS Catchment-CN utilizes the same parameterization as that in CLM4. The photosynthesis and transpiration depend non-linearly on solar radiation. The canopy is assumed to consist of sunlit leaves and shaded leaves, and the DRPAR and DFPAR absorbed by the vegetation is apportioned to the sunlit and shaded leaves as described by Thornton and Zimmermann (2007). The prognostic carbon storages underlying the phenological variables are computed as a matter of course along with values of canopy conductance that reflect an explicit treatment of photosynthesis physics. These canopy conductances, along with the LAIs diagnosed from the new carbon prognostic variables, are fed into the energy and water balance calculations in the original catchment LSM. The output fluxes from the merged system include carbon fluxes in addition to traditional fluxes of heat and moisture. The merger of the two models allows Catchment-CN to follow 19 distinct vegetation types. Koster and Walker (2015) have used Catchment-CN within an atmospheric global circulation model (AGCM) framework to investigate interactive feedback among vegetation phenology, soil moisture, and temperature. In this study, the modeled atmospheric CO_2 from the AGCM is used to drive the carbon, water, and energy dynamics in the Catchment-CN model.

In addition to the GEOS ESM, we use a photolysis scheme, FastJX, in its stand-alone mode to explore how incoming solar radiation penetrates the atmosphere in the presence of aerosols and clouds in order to enhance our basic understanding of the role of atmospheric particles on radiation. FastJX is based on the original Fast-J scheme, which was developed for tropospheric photochemistry with interactive consideration of aerosol and cloud impacts at 291–850 nm (Wild et al., 2000), and Fast-J2, which extended the scheme into the deep UV spectrum range of 177-291 nm (Bian and Prather, 2002).

2.2 Observational data
We mostly rely on the GoAmazon ("Green Ocean Amazon") field campaign (http://campaign.arm.gov/goamazon2014/) for in-situ aerosol observations to assess the model-simulated OA concentrations. GoAmazon is an integrated field campaign conducted in the central Amazon Basin (Martin et al., 2016). Specifically, the following datasets are used: a) the surface OA concentration measured in 2014 by the Aerosol Chemical Speciation Monitor (ACSM) operated by the Department of Energy's (DOE) Atmospheric Radiation Measurement (ARM) Mobile Facility located 70 km downwind of Manaus, Brazil (Ng et al., 2011), b) the surface CO volume mixing ratio in 2014 at Manaus measured by Los Gatos Research (LGR) N_2O/CO Analyzer that uses LGR's patented Off-axis Integrated Cavity Output Spectroscopy (ICOS) technology, and c) the vertical profile of OA concentration measured by a time-of-Flight Aerosol Mass Spectrometer (ToF-AMS) instrument on the ARM Aerial Facility Gulfstream-1 (G-1) aircraft during the dry season of 2014 (Sept 06-Oct 04, 2014) (Shilling et al., 2018). The G-1 aircraft was based out of the Manaus International airport and flew patterns designed to intersect the Manaus urban plume at increasing downwind distance from the city (e.g., 59-61°W and 4-2.5°S). In addition, we evaluate the model with AOD and single scattering albedo (SSA) measurements taken at a central Amazon station (Alta-Floresta) in the ground-based Aerosol Robotic Network (AERONET) sun photometer network (http://aeronet.gsfc.nasa.gov). We also

277 use MODIS collection 6.1 level-3 AOD product
278 (http://modis.gsfc.nasa.gov/data/dataprod/index.php), which is characterized by observations
279 with large spatial coverage.
280
281 MODIS cloud products (https://modis-atmosphere.gsfc.nasa.gov/data/dataprod/), specifically
282 total cloud fraction and cloud optical depth in liquid and ice particles, are used to evaluate the
283 model cloud simulation. We use the cloud data from MODIS collection 6.1 MYD08_D3, a level-
284 3 1°×1° global gridded monthly joint product derived from the MODIS level-2 pixel level
285 products. MODIS level 2 cloud fraction is produced by the infrared retrieval methods during
286 both day and night at a 5×5 1-km-pixel resolution. Level 2 cloud optical thickness used in this
287 study is derived using the MODIS visible and near-infrared channel radiances from the Aqua
288 platform.
289
290 The satellite-derived Clouds and the Earth's Radiant Energy System product CERES-EBAF is
291 used to evaluate the GEOS simulation of radiation fields. CERES-EBAF retrieves surface
292 downward shortwave radiation (R_{SFC}) using cloud information from more recent satellite data
293 (MODIS, CERES, CloudSat and CALIPSO) and aerosol fields from AERONET/MODIS
294 validation-based estimates (Kato et al., 2013). This global product is provided at a 1°×1°
295 horizontal resolution and covers the years 2000-2015 for both all- and clear-sky conditions. The
296 multiyear R_{SFC} products provide both a spatial and temporal view of radiation over Amazonia.

297 Two observation-based GPP products (FluxCom and FluxSat) are used to evaluate ecosystem
298 productivity in the GEOS simulations. The FluxCom GPP product provides globally distributed
299 eddy-covariance-based estimates of carbon fluxes between the biosphere and the atmosphere
300 through upscaling using machine learning methods (Jung et al., 2020). FluxSat GPP is estimated
301 with models that use satellite data (e.g., MODIS reflectances and solar-induced fluorescence
302 (SIF)) within a simplified light-use efficiency framework (Joiner et al., 2018). We use monthly
303 GPP for August through October of 2010-2015 in this study.

304   **2.3 Experiment setup**
305 All experiments were run with the coupled atmosphere and land components of the NASA
306 GEOS ESM system discussed above. The sea surface temperature (SST) for the atmospheric
307 dynamic circulation is provided by the GEOS Atmospheric Data Assimilation System (ADAS)
308 that incorporates satellite and in situ SST observations and assimilates Advanced Very High
309 Resolution Radiometer (AVHRR) brightness temperatures. The experiments were run in replay
310 mode, which means that the model dynamical variables (winds, pressure, temperature, and
311 humidity) were set, every 6 hours, to the values archived by the Modern-Era Retrospective
312 Analysis for Research and Applications version 2 (MERRA-2) meteorological reanalysis (Gelaro
313 et al. 2017); a 6-hourly forecast provided the dynamical and physical fields between the 6-hour
314 resets. In effect, the replay approach forces the atmospheric "weather" simulated in the model to
315 agree with the reanalysis. This nudging of the GEOS dynamic fields toward the MERRA2
316 reanalysis ensures that the atmospheric conditions of our four simulations (see below) remain
317 close to each other, allowing a more focused study of radiative impact on ecosystem. All
318 designed experiments were run over 2010-2016, a period that includes La Niña (2010-2011), El
319 Niño (2015-2016), and neutral years as indicated by the Oceanic Niño Index (ONI,
320 https://origin.cpc.ncep.noaa.gov/) (Figure S1). Information regarding long-term BB OA

321 emissions (i.e., 1997-2016) and long-term MERRA2 cloud fraction anomalies (i.e., 1995-2018)
322 is shown in Figure S2. The selected period of 2010-2016 represents well the long-term period in
323 terms of the variation of BB emissions and cloud coverage.
324
325 Our experimental design makes extensive use of GEOS's highly flexible configuration. First, the
326 GEOS GOCART module includes a tagged aerosol mechanism. Each specific aerosol
327 component in GOCART is simulated independently from the others, and the contribution of each
328 emission type to the total aerosol mass is also not interfered by that of other emission types.
329 Thus, additional aerosol tracers can easily be "tagged" according to emission source types. This
330 makes it possible for GOCART to calculate and transfer two sets of aerosol fields (e.g., one with
331 and one without a biomass burning source) to the radiation module. Second, the radiation module
332 can in turn calculate a set of atmospheric radiation fields corresponding to each set of aerosol
333 fields, and it can then disseminate both sets of radiation fields to the various components of
334 interest (i.e., cloud module, land ecosystem module, etc.) according to the needs of our
335 experiments (see below).
336
337 Table 1 provides a brief summary of the experiments performed for this study. First, we designed
338 a pair of experiments (allaer and nobbaer, hereafter referred to as "pair1") to explore the BBaer
339 DRFE on the land productivity via PAR (objective 1). The allaer and nobbaer experiments are
340 designed to simulate the same atmospheric dynamics but send different PAR fluxes into the
341 Catchment-CN model. Specifically, both the allaer and nobbaer experiments used all
342 atmospheric aerosols including real-time biomass burning emissions over 2010-2016 to calculate
343 a set of radiation fields (R^1) to drive atmospheric circulation; however, with the help of GEOS's
344 flexible configuration, the nobbaer experiment also calculated a second set of radiation fields
345 (R^2) that used non-BB aerosols only. R^1 was sent to Catchment-CN in the allaer experiment
346 whereas R^2 was sent to Catchment_CN in the nobbaer experiment. In this way, the only
347 difference between the allaer and nobbaer experiments was the PAR fluxes used to drive the
348 ecosystem model – only the PAR fluxes used in allaer reflected the presence of biomass burning
349 aerosols. The atmospheric meteorological fields in the two experiments, including clouds, skin
350 temperature, and soil moisture, show only minor differences stemming from land feedback
351 (Figure S3-4, Table 3, Table S1e and Table S2e). A negligible impact on cloud fields has also
352 been reported in Pedruzo-Bagazgoitia et al. (2017).
353
354 Table 1. Designed experiments (2010-2016) with their perturbation on aerosol fields and
355 subsequent impact on radiation and ecosystem

Exp Name		Aerosol	R in RRTMG	R driving Atmosphere	R driving Catchment-CN	Purpose
Pair 1	allaer	Standard all, w/ Realtime AERbb emission	R^1_{top}, R^1_{dir}, R^1_{diff} (all aerosol)	R^1_{top}, R^1_{dir}, R^1_{diff}	R^1_{dir}, R^1_{diff}	Check atmospheric BB aerosol impact on plants via radiation fields during 2010-2016
	nobbaer		R^1_{top}, R^1_{dir}, R^1_{diff} (all aerosol) R^2_{top}, R^2_{dir}, R^2_{diff} (all non-bb aerosol)	R^1_{top}, R^1_{dir}, R^1_{diff}	R^2_{dir}, R^2_{diff}	
Pair 2	callaer	Standard all, w/ AERbb emission fixed at 2010	R^1_{top}, R^1_{dir}, R^1_{diff} (all aerosol)	R^1_{top}, R^1_{dir}, R^1_{diff}	R^1_{dir}, R^1_{diff}	Check how clouds adjust the above impact
	cnobbaer		R^1_{top}, R^1_{dir}, R^1_{diff} (all aerosol) R^2_{top}, R^2_{dir}, R^2_{diff} (all non-bb aerosol)	R^1_{top}, R^1_{dir}, R^1_{diff}	R^2_{dir}, R^2_{diff}	

356
357

358 We also designed a pair of experiments (callaer and cnobbaer, hereafter referred to as "pair2") to
359 address the sensitivity of the BBaer DRFE to the presence of the Amazon dry season cloud fields
360 (objective 2). The pair2 experiments are similar to those in pair1 except that the particular BB
361 emissions of year 2010 were repeated during all seven years. Applying a fixed aerosol emission
362 allows us to attribute the interannual variation of the ecosystem solely to the influence of
363 interannual variations in atmospheric meteorological fields, including clouds. In addition,
364 combining the pair1 and pair2 experiments provides two biomass burning aerosol emissions for
365 each year except 2010, which allows us to compare the impacts of different emissions under
366 similar meteorological environments (Figure S3-4, Table 3, Table S1e and Table S2e). Please
367 note that the experiments in this study were intentionally designed to allow the aerosols to affect
368 the vegetation only through their impact on the direct and diffuse radiation that enters ecosystem
369 and not, for example, through their other potential impacts on the environment. Future study may
370 focus on these other impacts. Given that the experiment period covers strong La Niña and El
371 Niño years, we can examine BBaer impacts on ecosystem productivity under the full range of
372 Amazon background cloud fields.
373
374   **3.   Results and Discussion**
375
376   **3.1 Evaluation of GEOS simulations of aerosol, cloud, radiation, and ecosystem**
377   **response**
378 The NASA GEOS ESM model, including its aerosol, cloud, radiation, and ecosystem modules as
379 used in the baseline simulation (i.e., experiment allaer), has been evaluated extensively and
380 utilized in a number of scientific studies. However, very few of the past studies with GEOS was
381 concentrated on detailed model evaluation over South America. We provide such an evaluation
382 here.
383
384 The simulated tracer fields are compared with measurements over the Amazon in Figures 1 and
385 2. Figure 1 shows results for surface OA concentration, surface CO concentration, and the OA
386 concentration vertical profile. We focus primarily on the OA evaluation since it is the major
387 component of biomass burning aerosols. Figure 1a shows the comparison of surface daily OA
388 concentration between the model simulation and the GoAmazon measurements at Manaus,
389 Brazil, in 2014 (The location is indicated in Figure 2c with an open-diamond). The simulated OA
390 broadly captures the seasonal trend in OA concentrations measured at Manaus, but it is lower
391 than observed OA values by ~24% during Sept-Oct and ~ 30% annually. For the period of
392 interest, the model simulates a large fire signal in August that is not seen in the measurements.
393 However, this strong August biomass burning signal does show up in the CO measurements
394 (Figure 1b), which should also be from biomass burning. The reasons for such discrepancy from
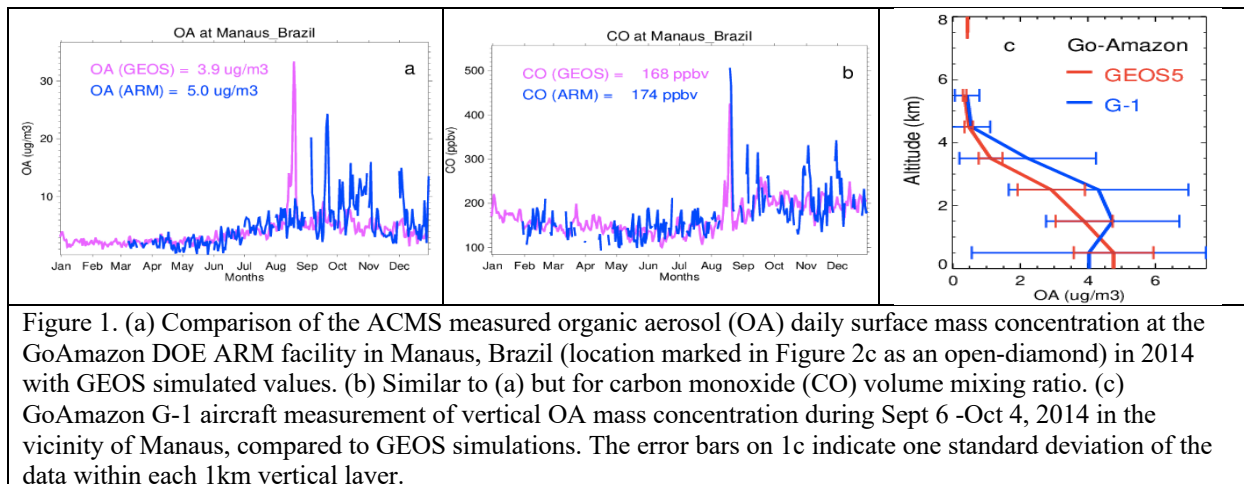395 observations are not clear.
396

Figure 1. (a) Comparison of the ACMS measured organic aerosol (OA) daily surface mass concentration at the GoAmazon DOE ARM facility in Manaus, Brazil (location marked in Figure 2c as an open-diamond) in 2014 with GEOS simulated values. (b) Similar to (a) but for carbon monoxide (CO) volume mixing ratio. (c) GoAmazon G-1 aircraft measurement of vertical OA mass concentration during Sept 6 -Oct 4, 2014 in the vicinity of Manaus, compared to GEOS simulations. The error bars on 1c indicate one standard deviation of the data within each 1km vertical layer.

397
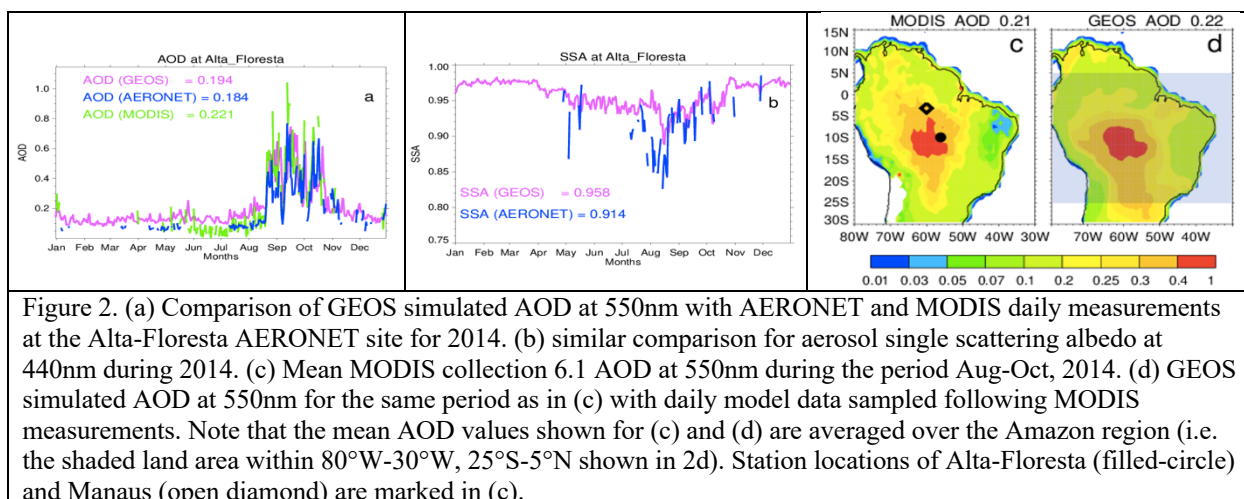
Figure 2. (a) Comparison of GEOS simulated AOD at 550nm with AERONET and MODIS daily measurements at the Alta-Floresta AERONET site for 2014. (b) similar comparison for aerosol single scattering albedo at 440nm during 2014. (c) Mean MODIS collection 6.1 AOD at 550nm during the period Aug-Oct, 2014. (d) GEOS simulated AOD at 550nm for the same period as in (c) with daily model data sampled following MODIS measurements. Note that the mean AOD values shown for (c) and (d) are averaged over the Amazon region (i.e. the shaded land area within 80°W-30°W, 25°S-5°N shown in 2d). Station locations of Alta-Floresta (filled-circle) and Manaus (open diamond) are marked in (c).
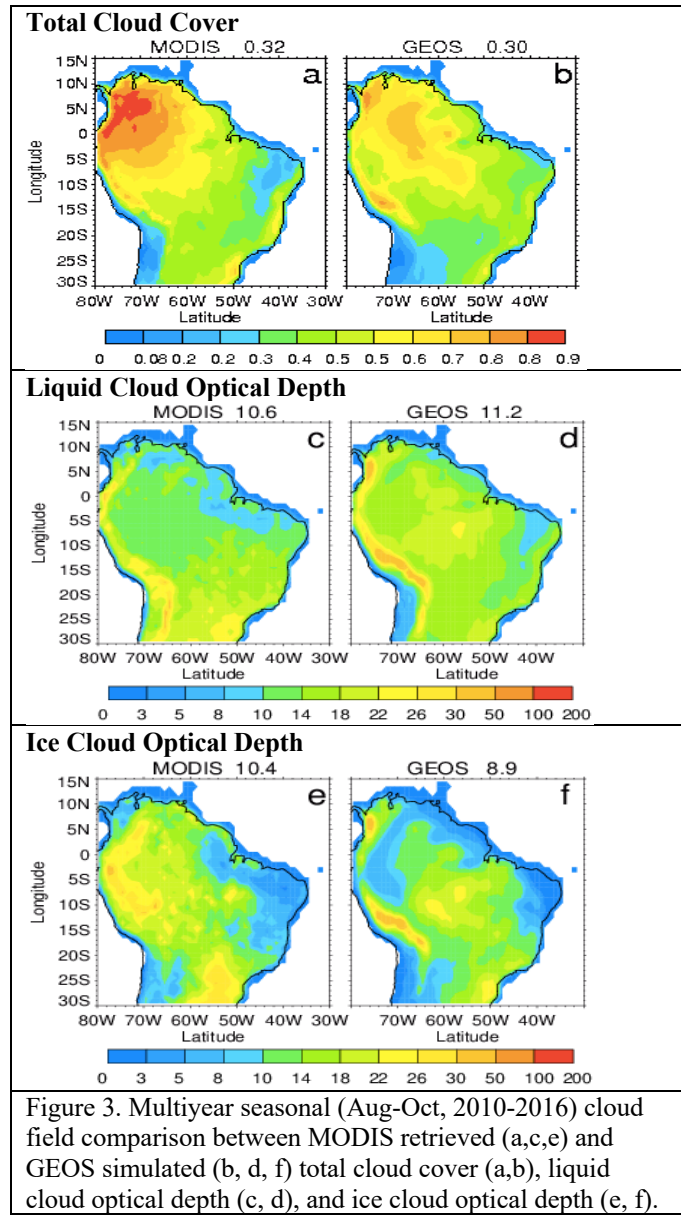
398

399 When compared with aircraft G-1 measurements over a ~2°×2° region around the center of
400 Manaus during the biomass burning season (Sept. 6 – Oct. 4, 2014) (Figure 1c), the simulated
401 vertical OA concentrations underestimate the measurements above 1 km altitude but
402 overestimate them under it, although they overlap within their standard deviations for all
403 altitudes. Here the model data have been sampled spatially and temporally along the G-1 flight
404 paths. This surface OA overestimation by the model seems to contradict the model's
405 underestimation seen in Figure 1a, indicating that capturing aerosols at the right times and
406 locations is a challenge.

407

408 Figure 2 shows the AOD (550nm) and SSA (440nm) comparison at the AERONET station of
409 Alta-Floresta, which is located close to the area of the most intensive Amazon fires (location is
410 marked in Figure 2c as a filled-in circle). The model-simulated, AERONET-measured, and
411 MODIS-retrieved AOD at this site agree within 20% (Figure 2a), all showing a peak of AOD
412 during the biomass burning season. SSA during the burning season generally ranges between
413 0.85 – 0.95 (Figure 2b). The model agrees with the measurements with accurate better than 5%
414 except during the first half of August, when the model aerosols are too scattering. However, it is
415 puzzling to observe the extremely low measured SSA in the beginning of August given that the
416 AOD is still low then, as shown in Figure 2a. It could be the quality of AERONET SSA is not
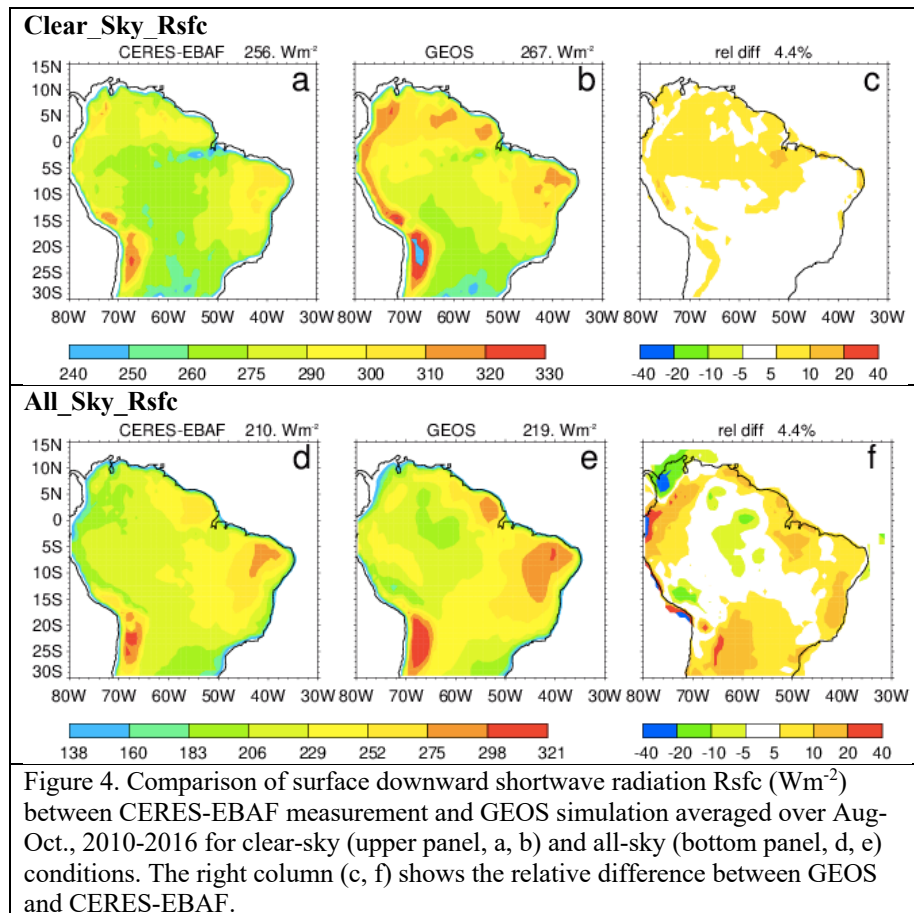
417   "reliable" at low AOD (Chin et al., 2009). Because of the low sensitivity to the absorption when
418   aerosol loading is low, SSA is retrieved with sufficiently high accuracy only when the
419   total AOD at 440 nm is equal or higher than 0.4 and solar zenith angle is 50 degree or higher
420   (Dubovik et al., 2000, 2002). Regionally over the Amazon region, defined throughout the study
421   as the land area within 80°W-30°W, 25°S-5°N (shaded land area in Figure 2d), the model-
422   simulated AOD (0.22 in Figure 2d) during the biomass burning season generally agrees with
423   MODIS satellite retrievals (0.21 in Figure 2c). A simulated high bias is seen over the east
424   Amazon; however, though this region is in our area of interest, the bias should have only a minor
425   impact on our study given that the area is relatively bare, with little vegetation coverage.
426
427
428
429
430
431
432
433
434
435
436

Figure 3. Multiyear seasonal (Aug-Oct, 2010-2016) cloud field comparison between MODIS retrieved (a,c,e) and GEOS simulated (b, d, f) total cloud cover (a,b), liquid cloud optical depth (c, d), and ice cloud optical depth (e, f).

461   The accurate simulation of cloud fields is also important for our study. In Figure 3 we evaluate
462   the GEOS-simulated cloud cover fraction and cloud optical depth with MODIS satellite

463 products. Here the GEOS data have been sampled with MODIS overpass time and location.
464 GEOS generally captures the magnitude and main features of the cloud fields observed in
465 MODIS, though with some differences; the model overestimates the cloud quantities over the
466 central Amazon and underestimates them in northwest South America. The overall difference
467 over the Amazon region between simulated and MODIS-based estimates is less than 7% for
468 cloud cover fraction, 10% for liquid water cloud optical depth, and 15% for ice cloud optical
469 depth. The seasonality of these cloud quantities is shown in Figure S5a-c to further evaluate the
470 model performance. The model has a better cloud simulation during the period of Aug-Oct,
471 which is the focus period of this study since Amazon fires occur periodically every year in this
472 season.
473
474 Figure 4 shows a comparison between the simulated downward shortwave radiation at the
475 surface and CERES-EBAF measurements averaged over Aug-Oct., 2010-2016 for both clear-sky
476 and all-sky conditions. The comparison of the time series of monthly mean shortwave radiation
477 during 2010-2016 over the Amazon region is shown in Figure S6. GEOS captures the observed
478 spatial patterns with ~4% high bias for both clear and all sky conditions over the Amazon region.
479

Figure 4. Comparison of surface downward shortwave radiation Rsfc (Wm^{-2}) between CERES-EBAF measurement and GEOS simulation averaged over Aug-Oct., 2010-2016 for clear-sky (upper panel, a, b) and all-sky (bottom panel, d, e) conditions. The right column (c, f) shows the relative difference between GEOS and CERES-EBAF.

480
481 Following the evaluation approach in Malavelle et al. (2019), we evaluate our model's ability to
482 simulate GPP on the global scale against FluxCom and FluxSat. As mentioned in section 2.2,
483 FluxCom GPP is derived from surface measurements of carbon fluxes whereas FluxSat GPP is
484 derived from satellite data. The comparison of global distribution of multiyear average GPP

(Figure 5) and zonal mean multiyear average GPP (Figure 6) show that GEOS captures the GPP global distribution seen in the observations, with a GPP peak in tropics. The model does show a second peak in middle latitudes of the Southern Hemisphere but misses the observed peak in the Northern Hemisphere subtropics.
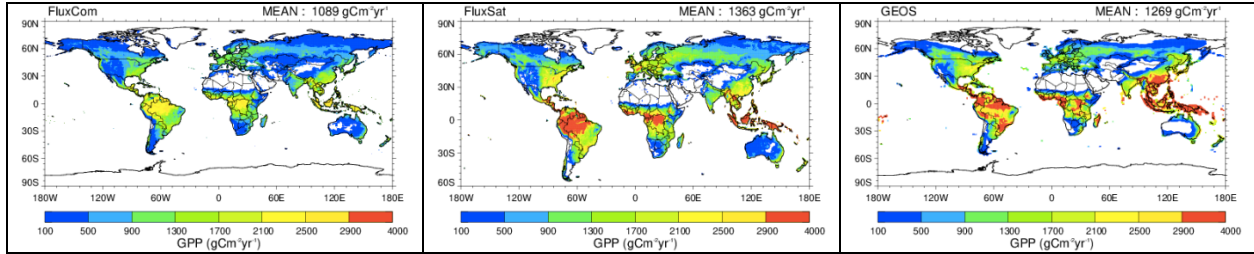

Figure 5. 2010-2015 multiyear average global GPP from FluxCom, FluxSat, and GEOS. The global average value is shown in the top.
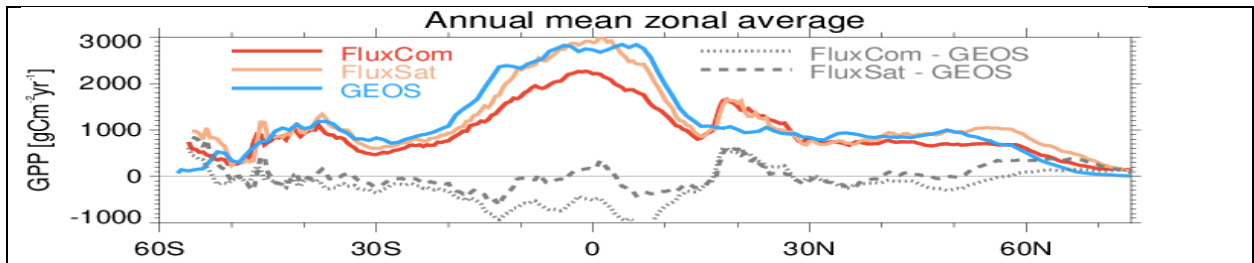

Figure 6. zonal mean of multiyear (2010-2015) average GPP from FluxCom, FluxSat, and GEOS.
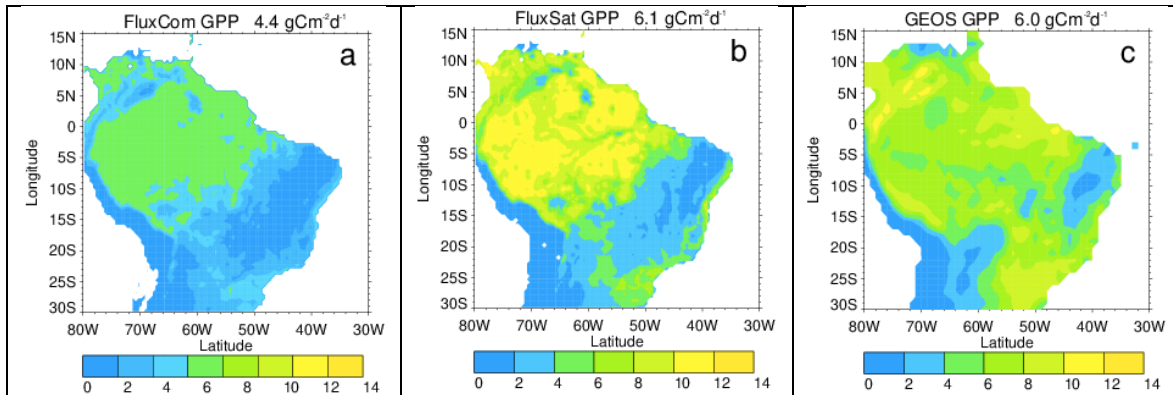

Figure 7. The multi-year (2010 – 2015) August – October mean Amazon GPP from (a) FluxCom (Jung et al., 2020), (b) FluxSat (Joiner et al., 2018) and (c) the GEOS ecosystem simulation with unit of gC m^{-2} day^{-1}. The Amazon regional average value is shown in the top.

Figure 7 shows GPP averaged over August to October of 2010-2015 from the two observations-based products and the GEOS simulation. The overall spatial distributions of GEOS GPP (Figure 7c) over South America show similar spatial pattern to both of the observations-based datasets (Figures 7a and 7b) with higher values over the eastern part of the domain but lying between the two datasets in other areas. Over the studied period and the Amazon region, the GEOS GPP is comparable to the FluxSat GPP and is about 35% higher than the FluxCom GPP.

501 The seasonality of GPP over the Amazon region from FluxCOM, FluxSat and GEOS during
502 2010-2015 is shown in Figure S7, and the corresponding time series of monthly means is shown
503 in Figure S8. During all four seasons, regional FluxCom GPP is the lowest and FluxSat GPP is
504 the highest. All datasets show higher GPP during Nov-Apr than during May-Oct. GEOS
505 multiyear annual average GPP is close to that of FluxSat but is higher than that of FluxCom.
506 Although there are few of observation sites available in FLUXNET 2015 Tier 1
507 (https://fluxnet.org/data/fluxnet2015-dataset/), Joiner et al. (2018) evaluated FluxSat GPP
508 performance around Amazonia using the flux tower measurements, which showed that the high
509 GPP values produced by FluxSat were supported by the flux tower values (Joiner et al., 2018).
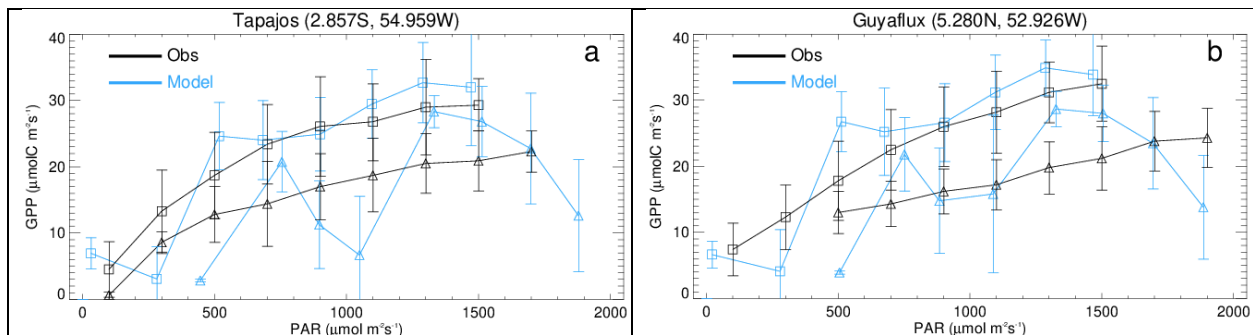
510

Figure 8. Observed (black) and GEOS modeled (blue) response of GPP to direct (triangles) and diffuse (squares) photosynthetically active radiation (PAR) averaged over bins of 200 µmol quanta m^2 s^{-1} at (a) Tapajos and (b) Guyaflux. Error bars show 1 standard deviation of all values within a bin. The observation data, representing the period 2002-2005 for Tapajos and 2006-2007 for Guyaflux, are taken from Figure 2 of Rap et al. (2015), whereas the model period is 2010-2016 for both sites.

511
512 Although the evaluations of global and regional multiyear average GPP conducted above
513 (Figures 5-7) are needed for the examination of the model's fundamental mechanisms including
514 photosynthesis, a more direct evaluation to address the model's accuracy in simulating observed
515 GPP response to changes in diffuse and direct surface radiation is shown in Figure 8. Following
516 the evaluation approach of Rap et al., (2015), we compared the GPP response to direct and
517 diffuse light at two Amazon sites, Tapajos and Guyaflux. The figure clearly demonstrates that in
518 the model, as in observations, diffuse light is more efficient in stimulating GPP.
519
520   **3.2 Principle of aerosol and cloud impact on surface downward radiation**
521 Radiative responses to aerosols and cloud fields are nonlinear. To better explain the phenomenon
522 examined here – that plant growth increases at low-to-intermediate AOD but decreases at high
523 AOD – we ran the column version of a radiation model, fast-JX (Wild et al., 2000; Bian and
524 Prather, 2002). Fast-JX solves the 8-stream multiple scattering in atmospheric solar radiation
525 transfer for direct and diffuse beams, using the exact scattering phase function and optical depths
526 of atmospheric molecules, aerosols, and clouds, and provides photolytic intensities accurate
527 typically to better than 3%, with worst case errors of no more 10% over a wide range of
528 atmospheric conditions (Wild et al., 2000). No special approximations are needed to treat
529 strongly forward-peaked phase functions. The model has also been evaluated against various
530 other models that participated in an international multi-model comparison for solar fluxes and
531 photolysis calculation (PhotoChem-2008 in Chipperfield et al., 2010) and against the
532 measurements from actinic flux spectroradiometers during the Atmospheric Tomography

533 (ATom) mission (Hair et al., 2018). In the aforementioned evaluations, the fast-JX model is
534 among the models with good performance. The model calculations provide three ratios: (i) CIdir,
535 the ratio of direct downward solar radiation at the surface (Rdir@srf) to the incoming total solar
536 radiation flux at the top of the atmosphere (Rtot@toa), (ii) CIdiff, the ratio of the downward
537 diffuse solar radiation flux (Rdiff@srf) to Rtot@toa, and (iii) CI, the ratio of total solar radiation
538 at the surface to Rtot@toa. Note that all Rs are for the 400-700 nm spectral band. Results for
539 different biomass burning AODs (including the clean air condition, where AOD = 0) for cloud-
540 free conditions are shown in Figure 9a. When the sky is clear and clean (both cloud-free and
541 without aerosols), roughly 90% of the incoming solar radiation at the top of the atmosphere can
542 reach the plant canopy (i.e., CIdir + CIdiff ≈ 0.9 at BBAOD = 0). The direct solar flux decreases
543 rapidly as the atmosphere becomes polluted (i.e., as BBAOD increases), but for BBAOD levels
544 less than ~0.75, the diffuse solar flux increases. The two are equivalent at AOD ~ 0.5. This light
545 redistribution from direct to diffuse can significantly stimulate plant photosynthesis given that
546 plants use diffuse light more efficiently. Ecosystems could still respond positively to the increase
547 of BBAOD even if the incident diffuse radiation decreases below its peak value, though for some
548 value of BBAOD, the reduction in total radiation will be large enough to overwhelm the impact
549 of increased diffuse radiation, and plant photosynthesis will be lower than that for clean sky
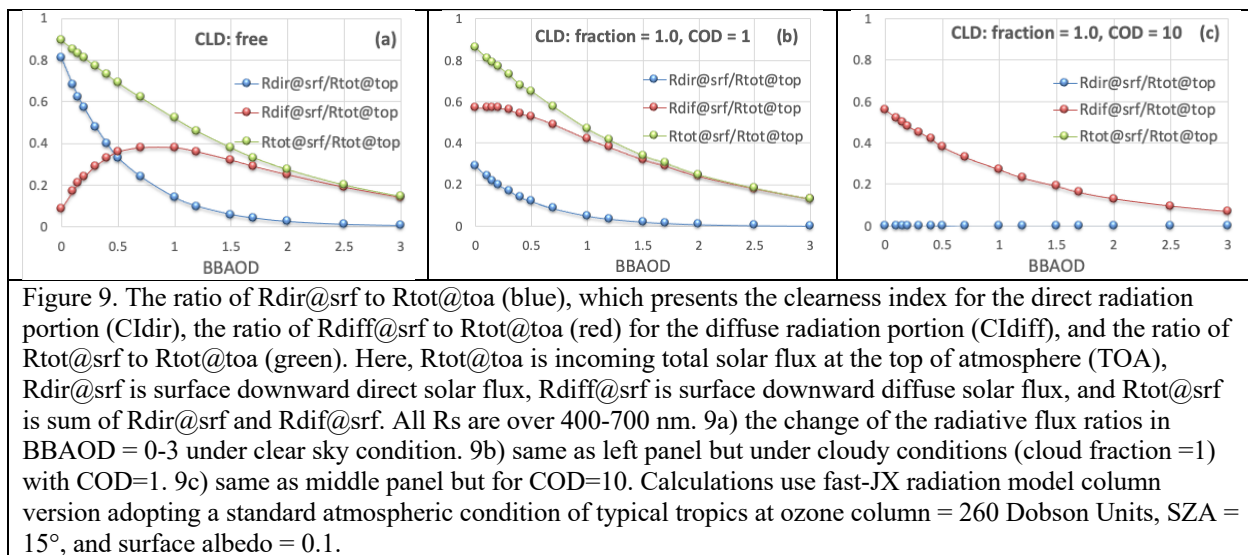550 conditions.
551

Figure 9. The ratio of Rdir@srf to Rtot@toa (blue), which presents the clearness index for the direct radiation portion (CIdir), the ratio of Rdiff@srf to Rtot@toa (red) for the diffuse radiation portion (CIdiff), and the ratio of Rtot@srf to Rtot@toa (green). Here, Rtot@toa is incoming total solar flux at the top of atmosphere (TOA), Rdir@srf is surface downward direct solar flux, Rdiff@srf is surface downward diffuse solar flux, and Rtot@srf is sum of Rdir@srf and Rdif@srf. All Rs are over 400-700 nm. 9a) the change of the radiative flux ratios in BBAOD = 0-3 under clear sky condition. 9b) same as left panel but under cloudy conditions (cloud fraction =1) with COD=1. 9c) same as middle panel but for COD=10. Calculations use fast-JX radiation model column version adopting a standard atmospheric condition of typical tropics at ozone column = 260 Dobson Units, SZA = 15°, and surface albedo = 0.1.
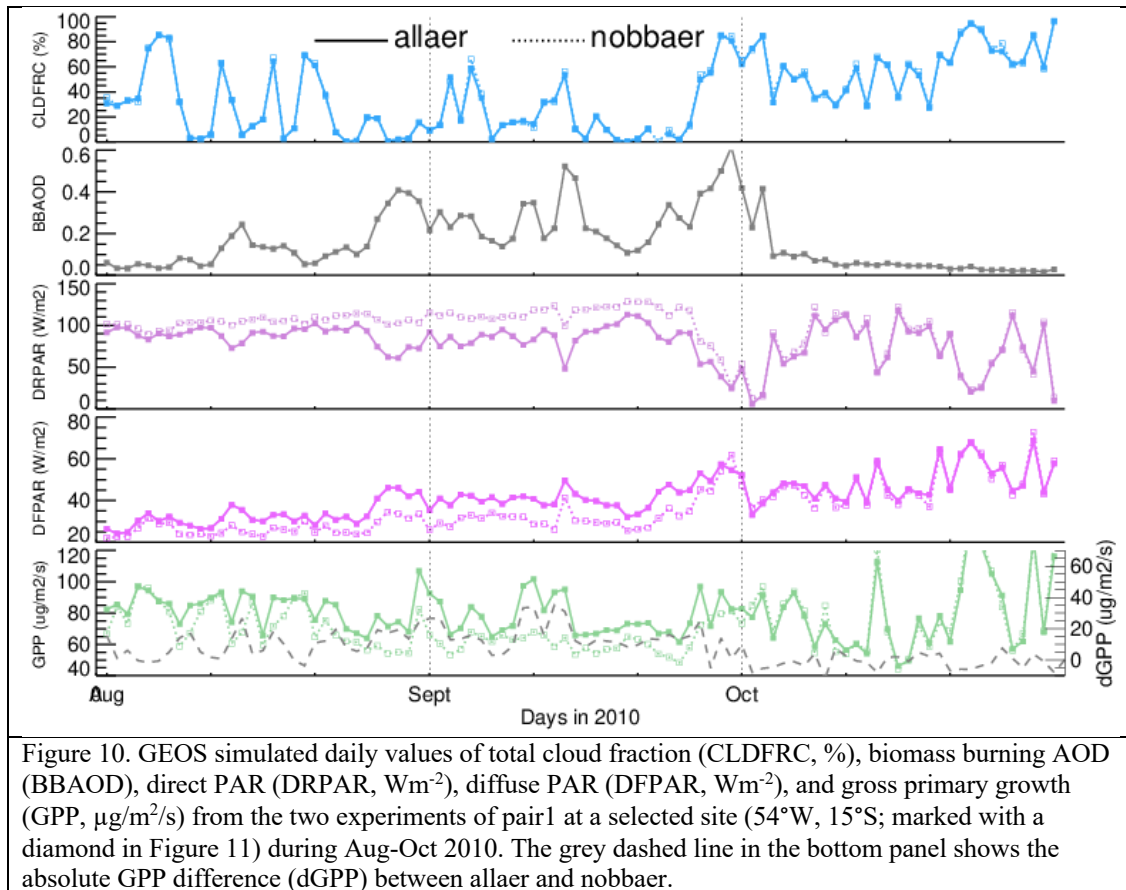
552
553 The Amazon dry season is characterized by high biomass burning aerosol loading combined with
554 low cloud cover, a good match to obtain more diffuse radiation without the loss of too much total
555 radiation. However, as we have pointed out, cloud impacts on radiation typically dominate those
556 of aerosols. To examine this, we repeated the radiation model calculations after adding, at the top
557 of the aerosol layer (~3.5km), a cloud layer with a cloud fraction of 1.0 and a cloud optical depth
558 (COD) of 1 (Figure 9b) and 10 (Figure 9c). The latter COD is close to the mean liquid cloud
559 COD over the Amazon dry season (Figure 3). The impact on Rdir@srf and Rdiff@srf is quite
560 large even with a very thin overhead cloud (Figure 9b). Without BBaer, the clouds already
561 produce abundant diffuse light that can reach the surface (i.e., CIdiff > 50%, as seen in both
562 Figure 9b-c), while almost shutting down the direct light (i.e., CIdir < 1% in Figure 9c).
563 Accordingly, for full cloud coverage, a clean sky (i.e., no aerosols) would provide the best
564 conditions for plant growth. When fires start, the diffuse light declines rapidly, reducing the

565 potential for plant growth. At BBAOD ~ 3 the ratios among Figure 9a-c look similar, that is,
566 essentially very little radiation reaches the surface.

567 The simple examples in Figure 9 illustrate the complicated responses of direct and diffuse light
568 to the presence of aerosol and cloud. Measurements indicate that plant growth peaks for a
569 clearness index (CI, defined as CIdir+CIdiff) of about 0.4-0.7 for some forest ecosystems (Butt
570 et al., 2010, Letts and Lafleur, 2005). This CI range translates, based on Figure 9, to a BBAOD
571 range of about 0.3~1.5 in clear sky and 0~0.5 in cloudy-sky conditions.
572
573 **3.3 How the ecosystem responds to the BBaer diffuse radiation fertilization effect**
574

Figure 10. GEOS simulated daily values of total cloud fraction (CLDFRC, %), biomass burning AOD (BBAOD), direct PAR (DRPAR, Wm^{-2}), diffuse PAR (DFPAR, Wm^{-2}), and gross primary growth (GPP, μg/m^2/s) from the two experiments of pair1 at a selected site (54°W, 15°S; marked with a diamond in Figure 11) during Aug-Oct 2010. The grey dashed line in the bottom panel shows the absolute GPP difference (dGPP) between allaer and nobbaer.
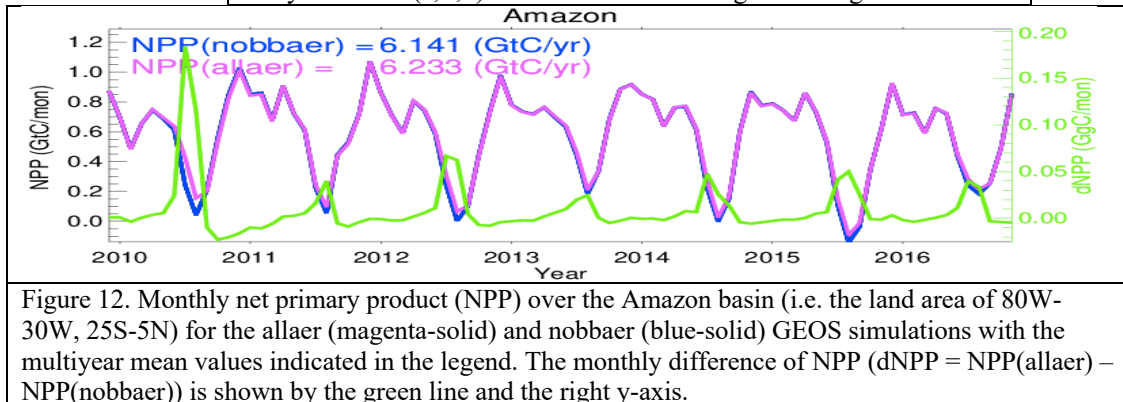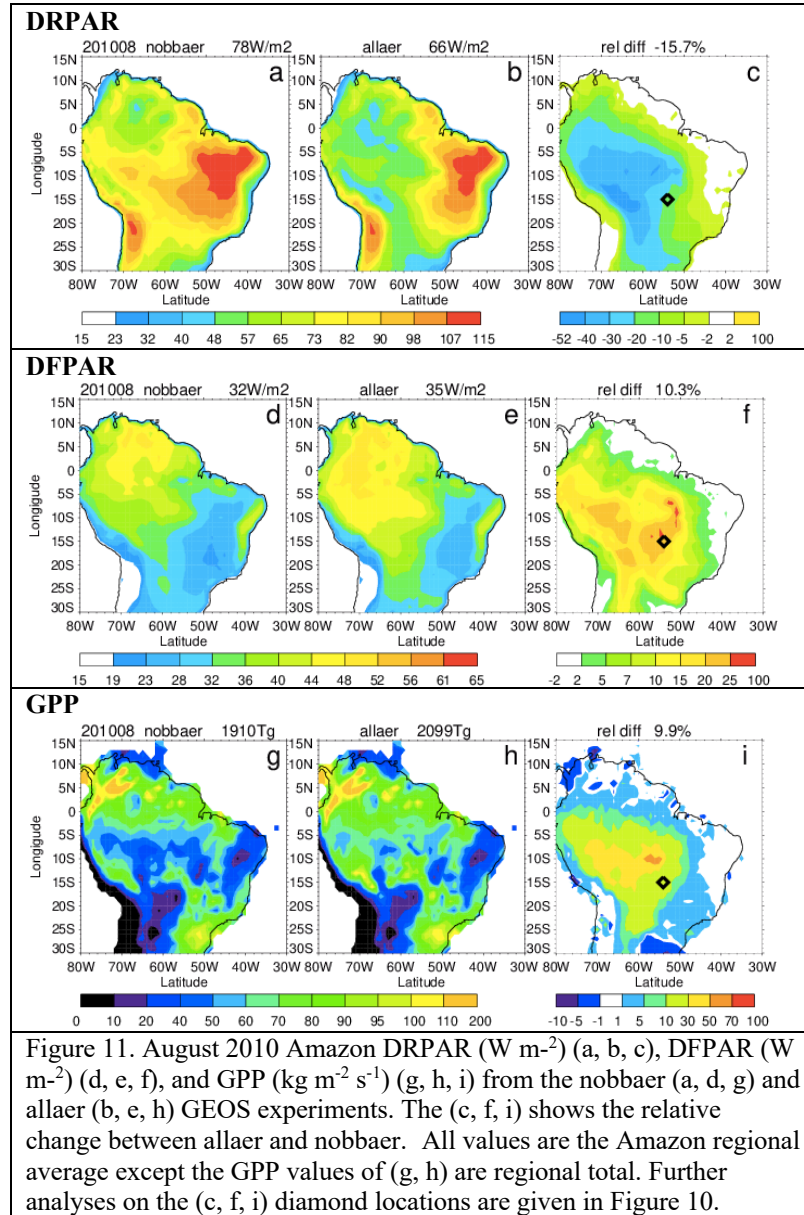
575
576 We first examine the two experiments in pair1 by taking a close look at the time series of
577 aerosol, cloud, radiation, and ecosystem responses generated at a selected site (54°W, 15°S)
578 during Aug-Oct 2010 (Figure 10) (site location marked in Figure 11), with the aim of extending
579 the general understanding gained in section 3.2 to a real case study at a single site in the
580 Amazon. This is an interesting site and period, showing a large DFPAR change (Figure 11f) and
581 providing a wide variety of conditions for study – the sky alternates between clear and cloudy
582 conditions in August, is relatively clear in September but relatively cloudy in October, and the
583 biomass burning aerosols increase in August, peak in September, and diminish greatly in early
584 October (Figure 10). During August-September, when the atmosphere experiences biomass
585 burning pollution, the allaer (with BBAOD light fertilizer) and nobbaer (without BBAOD light
586 fertilizer) results differ significantly: DRPAR for allaer (solid line) lies below that for nobbaer

587   (dotted-line), while DFPAR and GPP for allaer are generally higher than those for nobbaer. In
588   October, the sky is almost clean (i.e., low BBaer), leading to very similar results for DRPAR,
589   DFPAR, and GPP between the two experiments. Looking closer, we see that the changes of
590   DRPAR, DFPAR, and GPP between allaer and nobbaer are more prominent when the
591   atmosphere has low cloudiness and high aerosol (e.g., at the end of August), confirming both that
592   BBaer does transform some of the direct light at the surface into diffuse light and that plants are
593   more efficient in their use of diffuse light. When both cloudiness and aerosols are high (e.g., at
594   the end of September), the influence of aerosols is overwhelmed by clouds, and the impact of the
595   aerosols on radiation and the ecosystem becomes secondary.
596
597   We now evaluate BB aerosol impacts on radiation and ecosystem fields over the Amazon during
598   August 2010, when the aerosol has its largest impact. Figure 11 shows the simulated Amazon
599   DRPAR, DFPAR, and GPP fields from the two experiments comprising pair1 (nobbaer and
600   allaer). The distribution of DRPAR shows a clear spatial gradient, with low values in the
601   northwest and high values in the southeast, and the spatial pattern of DFPAR shows the reverse
602   pattern. These features are primarily controlled by the cloud distribution (Figure 3). Comparing
603   the nobbaer and allaer results by calculating field relative change (i.e., (allaer-nobbaer)/allaer),
604   we find that BBaer decreases DRPAR by 16% and increases DFPAR by 10% over the Amazon
605   region, with maximum local changes of up to -50% for DRPAR and 25% for DFPAR.
606   Interestingly, these maxima are not co-located, though the spatial patterns of perturbations do
607   agree with each other. The mismatch in the locations of the maxima in the difference fields
608   implies a nonlinear response of direct and diffuse light to aerosol and cloud particles (see section
609   3.2). In response to the inclusion of BBaer, the Amazon GPP increases by 10%. That is, the
610   increase in GPP stemming from the increase in the diffuse light fraction overwhelms a potential
611   reduction in GPP from a reduction of total PAR. When we consider all burning seasons over the
612   7-year studied period, the biomass burning aerosol increases DFPAR by 3.8% and decreases
613   DRPAR by 5.4%, allowing it to increase Amazon GPP by 2.6%. However, the 7-year averaged
614   GPP increases by 0.99% (Table 2), which is much less than the value during burning seasons.
615
616   We also examine the multi-year (2010-2016) BBaer impacts on net primary production (NPP),
617   that is, the rate at which carbon is accumulated (GPP) in excess of autotrophic respiration. In
618   essence, NPP can be considered a proxy for the net plant sink of atmospheric carbon. Figure 12
619   shows monthly and long-term averaged NPP over the Amazon Basin from the two experiments
620   comprising pair1. The monthly change of NPP (i.e., dNPP = NPP(allaer) – NPP(nobbaer)) is
621   shown in the figure as a green line. Each year, during the August-September period when BBaer
622   is high and cloudiness is low over the Amazon, BBaer is seen to enhance NPP. The percentage
623   difference of annually-averaged NPP (dNPP/NPP(nobbaer)*100) in % is 4.2, 0.06, 1.9, 0.5, 1.3,
624   1.9, and 1.0 for the seven studied years. That means the BBaer-induced NPP increases range
625   from 5 TgC yr^{-1} or 0.06% (2011) to 278 TgC yr^{-1} or 4.2% (2010), with a seven-year average of
626   92 TgC or 1.5%. This is equivalent to storing 92TgC annually within the Amazon ecosystem
627   during the studied period. The CO_2 fire emission data from the GFED4.1s emission inventory
628   indicate that over this area and time period, fires emit ~250TgCyr^{-1}. The NPP enhancement due
629   to the BBaer-induced diffuse sunlight fertilization thus compensates for about 37% of carbon
630   loss by fires.
631
632

DRPAR

DFPAR

GPP

Figure 11. August 2010 Amazon DRPAR (W m^{-2}) (a, b, c), DFPAR (W m^{-2}) (d, e, f), and GPP (kg m^{-2} s^{-1}) (g, h, i) from the nobbaer (a, d, g) and allaer (b, e, h) GEOS experiments. The (c, f, i) shows the relative change between allaer and nobbaer. All values are the Amazon regional average except the GPP values of (g, h) are regional total. Further analyses on the (c, f, i) diamond locations are given in Figure 10.

Figure 12. Monthly net primary product (NPP) over the Amazon basin (i.e. the land area of 80W-30W, 25S-5N) for the allaer (magenta-solid) and nobbaer (blue-solid) GEOS simulations with the multiyear mean values indicated in the legend. The monthly difference of NPP (dNPP = NPP(allaer) – NPP(nobbaer)) is shown by the green line and the right y-axis.

635 To assess how our simulated GPP/NPP response compares with other existing model estimates,
636 we summarize all relevant studies in Table 2. In addition to differences in model formulations of
637 fundamental physical mechanisms, these studies also differ in model simulation configuration
638 (e.g., online vs offline, freeGCM vs Replay), BB emission inventory, and study period. Although
639 our estimates of the increases in NPP across the Amazon region have a wide interannual
640 variation (ranging from 0.5 to 4.2%), our 7-year averaged NPP increase (1.5%) is close to the
641 value (1.4%) reported by Rap et al. (2015). Both studies considered only aerosol DRFE with
642 cloud presence. The NPP can be increased up to 52% in the burning season under clear-sky
643 conditions (Moreira et al., 2017). By accounting for the feedback from aerosol-climate
644 adjustments, the influence of aerosol on GPP/NPP is further increased (Malavelle et al., 2019;
645 Strada et al., 2016).
646
647 Table 2: Summary of model estimation of GPP increase in response to biomass burning aerosol
648 over Amazon Basin

Study	This work	Malavelle2019	Moreira2017	Rap2015	Strada2016
GPP	1.0% (dir+dif)		27% (dir+dif)	0.7% (dir+dif)	3.4% (dir+dif+clm))
NPP	1.5% (dir+dif)	1.9 to 2.7% (dif+dir+clm) 1.5 to 2.6% (dif) -1.2 to -2.5% (dir) 1.6 to 2.4% (clm)	52% (dir+dif)	1.4% (dir+dif)	
Period	Annual average over 2010-2016	Annual average over 30 model years, 2000 climate,	Sept., 2010 under cloud-free condition	Annual average over 1998-2007	Annual average over 30 model years, 2000 climate
Atmospheric Model	GEOS ESM	HadGEM2-ES	BRAMS		ModelE2 ESM
Running mode	replay	freeGCM	Regional model with ICBC from NCEP	offline	freeGCM
Vegetation model	Catchment-CN (using LSM4 for photosynthesis)	JULES	JULES	JULES	YiBs
Radiation model	RRTMG_SW	SOCRATES	CARMA	A two-stream radiative transfer model (Edwards and Slingo, 1996)	k-distribution approach with various updates (Schmidt et al., 2014)
Cloud model	Cloud microphysics model (Barahona et al., 2014)			Monthly mean clouds from ISCCP-D2	a mass flux cumulus parameterization (Del Genio and Yao, 1993)
Aerosol model	GOCART	CLASSIC	CCATT	GLOMAP	OMA
BB emission	GFED4s	GFEDv2 1997-2006 average	3BEM	GFED3	IPCC AR5

649 dir, dif, and clm represent for direct radiation, diffuse radiation, and climate adjustment, respectively
650 3BEM: the Brazilian Biomass Burning Emission
651 BRAMS: Brazilian developments on the Regional Atmospheric Modeling System
652 CARMA: the Com-munity Aerosol and Radiation Model for Atmospheres
653 CCATT: a Eulerian transport model suitable to simulate trace gases and aerosols
654 CLASSIC: the Coupled Large-scale Aerosol Simulator for Studies In Climate
655 GLOMAP: The 3-D GLObal Model of Aerosol Processes Model
656 HadGEM2-ES: The Hadley Centre Global Environment *Model*, version 2-Earth System
657 IPCC AR5: The Intergovernmental Panel on Climate Change Fifth Assessment Report
658 ISCCP-D2: the International Satellite Cloud Climatology Project
659 JULES: the Joint UK Land Environment Sim-ulator v3.0
660 OMA: One-Moment Aerosol,
661 SOCRATES: Suite Of Community RAdiative Transfer codes based on Edwards and Slingo
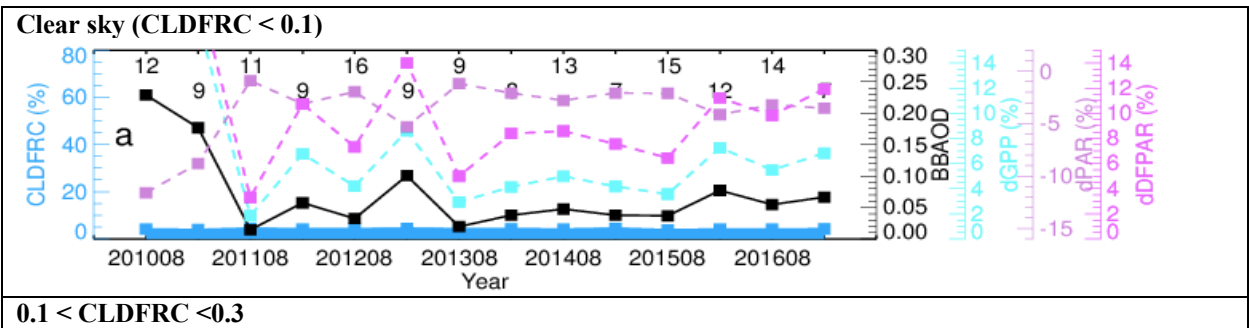662 YIBs: The Yale Interactive Terrestrial Biosphere model
663
664
665
666 **3.4 How clouds adjust the BBaer diffuse radiation fertilization effect**
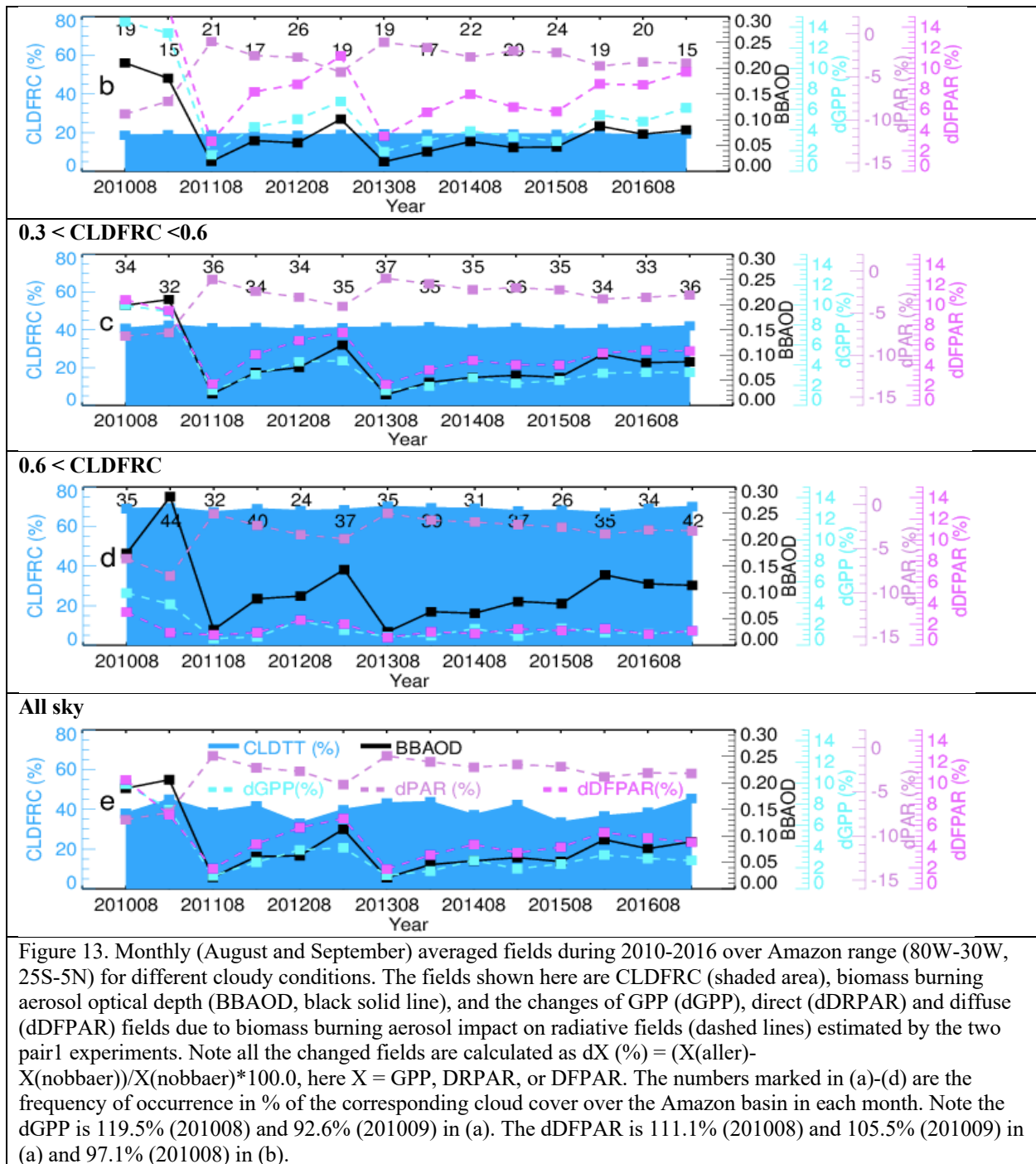
667 Our second objective in this study is to investigate how the presence of clouds modulates the
668 ability of BBaer to affect GPP. We highlight the cloud impact because even at the same biomass
669 burning aerosol optical depth (BBAOD), the surface downward DRPAR and DFPAR can be
670 very different between cloudy and cloud-free conditions (see section 3.2). As mentioned above,
671 the Amazon's so-called "dry season" still features a considerable amount of cloud, and the
672 cloudiness levels vary significantly from year to year. This raises some questions: How do
673 clouds affect the aerosol impact on radiation fields during the Amazon biomass burning season?
674 Could different levels of background clouds have different impacts on the efficacy of the BBaer
675 DRFE? There are two distinctive features in clouds and aerosols that require us to treat them
676 differently in their impact on the radiation flux to the ecosystem. First, like our distinction of
677 natural and anthropogenic aerosols in their impact on air quality and climate, the cloud is a more
678 natural phenomenon, while biomass burning aerosols (BBaer) can be, at least partially,
679 controlled by humans. Second, clouds are much more efficient in controlling both direct and
680 diffuse radiation fields than aerosol (Figure 6). What is the potential range of the variation of
681 Amazon clouds in burning seasons when the Amazon experiences environments of La Niña,
682 normal years, and El Niño? To what extent does this range of cloud variation adjust the
683 efficiency of "diffuse radiation fertilization effect" under the same emission strategy? These
684 questions were not addressed clearly in previous studies, and we have tried to answer these
685 questions in this study. Here, to quantify the cloud influence, we examine BBaer impacts during
686 clear-sky (cloud cover < 0.1), cloudy-sky (cloud cover 0.1-0.3, 0.3-0.6 and >0.6), and all-sky
687 conditions based on GEOS gridded daily cloud cover over the Amazon region as shown in
688 Figure 13.
689
690 Generally, the curves for BBAOD (solid black line) and dGPP (dashed light-blue line) are
691 strongly and positively correlated, from R = 77.4% for cloud cover > 0.6 (Figure 13d) to R >
692 94.5% for the four other cloudiness conditions (Figure 13a-c, e). This indicates that interannual
693 changes in dGPP are primarily controlled by interannual fluctuations of biomass burning
694 aerosols. The correlation presumably stems from the fact that biomass burning aerosols increase
695 the diffuse PAR reaching the canopy (dashed pink line) although they decrease the total PAR
696 (dotted purple line) via decreasing direct PAR (Table 3 and Table S1a). This aerosol-radiation-
697 GPP relationship is seen to vary with cloud amount with clouds acting to reduce the aerosol
698 impact; both the diffuse radiation and the GPP show larger changes with BBAOD under clear
699 sky conditions. The overall (i.e., all-sky) aerosol impact on dGPP is similar to that for a cloud
700 coverage of 0.3-0.6, simply because the averaged cloud coverage over the Amazon during the
701 studied period is roughly in that range.
702
703

Clear sky (CLDFRC < 0.1)

0.1 < CLDFRC <0.3

20

Figure 13. Monthly (August and September) averaged fields during 2010-2016 over Amazon range (80W-30W, 25S-5N) for different cloudy conditions. The fields shown here are CLDFRC (shaded area), biomass burning aerosol optical depth (BBAOD, black solid line), and the changes of GPP (dGPP), direct (dDRPAR) and diffuse (dDFPAR) fields due to biomass burning aerosol impact on radiative fields (dashed lines) estimated by the two pair1 experiments. Note all the changed fields are calculated as dX (%) = (X(aller)-X(nobbaer))/X(nobbaer)*100.0, here X = GPP, DRPAR, or DFPAR. The numbers marked in (a)-(d) are the frequency of occurrence in % of the corresponding cloud cover over the Amazon basin in each month. Note the dGPP is 119.5% (201008) and 92.6% (201009) in (a). The dDFPAR is 111.1% (201008) and 105.5% (201009) in (a) and 97.1% (201008) in (b).

704

705 Figure 13 and Table S1e show that on an interannual (dry season) basis, the aerosol DRFE
706 differed the most between 2010 and 2011 (i.e., the dGPP was 8.7% in 2010 and 1.8% in 2011).
707 During these two years, the average cloud fractions (CLDFRC) are similar, 42% in 2010 and
708 41% in 2011, but BBAOD decreased significantly, by about 80% from 0.198 in 2010 to 0.042 in
709 2011. Thus, although cloudiness does temper the impact of aerosols on radiation and the
710 ecosystem, the interannual variation of the aerosol DRFE is primarily controlled by variations in
711 biomass burning aerosols (e.g., > 6 times variation of biomass burning emissions and BBAOD,

21

712 table S1e). In addition to the detailed information given in Tables S1a-e and S2a-e, we
713 summarize in Table 3 the averaged GPP, DFPAR, DRPAR, CLDFRC, and BBAOD during Aug-
714 Sept, 2011-2016 over the Amazon region in all-sky conditions. Also given in Table 3 is the
715 multi-year (2011-2016) averaged GPP over the Amazon region from all four simulations.
716
717 Table 3. Summary of mean GPP, DRPAR, DFPAR, CLDFRC and BBAOD over Aug-Sept of
718 2011-2016, as well as the relative changes of GPP, DRPAR, DFPAR and CLDFRC within a pair
719 of simulations.

pair	experiment	GPP	DRPAR	DFPAR	CLDFRC	BBAOD
		GtC/Amazon	Wm^{-2}	Wm^{-2}		
Pair1	allaer	1.88	72.5	36.8	0.395	0.062
	nobbaer	1.84	76.5	35.3	0.395	
	Diff (%)	2.5	-5.3	4.1	0	
Pair2	callaer	1.96	64.5	38.0	0.396	0.212
	cnobbaer	1.83	75.4	35.1	0.395	
	Diff (%)	6.9	-14.4	8.2	0	

720
721 Recall, the pair2 experiments are equivalent to the pair1 experiments except for using the 2010
722 BB emissions for every year during 2011-2016. By jointly analyzing pair1 and pair 2, we can
723 quantify the impacts of two different sets of BB emissions during the study period. This is, in
724 principle, similar to the method of aerosol radiative forcing (RF) estimation (i.e., estimating
725 aerosol radiative effect (RE) with and without aerosol for present-day (pair1) and pre-industrial
726 (pair2) conditions and then deriving RF as a difference between the two pair REs). Here we
727 study the sensitivity of the aerosol DRFE to a unit change of AOD. We call it susceptibility of
728 the DRFE to BB aerosols. That is, on a daily basis, the sensitivity of a variable X to a change in
729 the biomass burning AOD is calculated as: $ddX/dAOD = ((dX)_1-(dX)_2)/(AOD_1-AOD_2)$. Here, the
730 X represents GPP, DRPAR, and DFPAR, and the subscripts 1 and 2 represent the pair1 or pair2
731 experiment, respectively.
732
733 ddX/dAOD is computed on a gridded daily basis over August-September of 2011-2016. The
734 calculations are then catalogued according to daily cloud cover fraction – we combine the results
735 within each of 10 cloud fraction bins (0-0.1, 0.1-0.2, …, 0.9-1.0). To examine the maximum
736 impact of interannual cloud change during our study period, the binned ddX/dAOD vs. CLDFRC
737 relationship is also computed separately from daily (August-September) values in 2013 and from
738 corresponding daily values in 2015, as these are the years for which monthly cloud cover is
739 around the maximum (0.44) and minimum (0.35), respectively (Figure 13 and table S1e).

740 Figure 14 shows the results. An almost linear relationship is seen between the ddX/dAOD values
741 and cloud cover fraction. BB aerosols increase GPP in clear sky conditions (e.g., 29.6 $kgm^{-2}s^{-1}$)
742 but decrease it under full cloudiness conditions (e.g., -5.8 $kgm^{-2}s^{-1}$). The cloud fraction at which
743 BB aerosol switches from stimulating to inhibiting plant growth occurs at ~0.8. Cloud conditions
744 thus not only affect strongly the strength of the aerosol DRFE but can also change the
745 fundamental direction of the effect. The lines produced for the three different study periods are
746 fairly similar, indicating that the relationship of ddX/dAOD to CLDFRC is fairly stable within
747 the range of cloud cover seen over the Amazon during the period of interest. Figure 14 also
748 indicates that the dGPP can change from 18.5 to 15.5 ($kgm^{-2}s^{-1}$) with a unit AOD of burning
749 particles released to the atmosphere under the range of Amazon interannual cloud variation in
750 dry season, which is 0.35 to 0.44 in our study period. In other words, there is ~20% dGPP

751 uncertainty adjusted by background Amazon cloud. Our work demonstrates quantitively the role
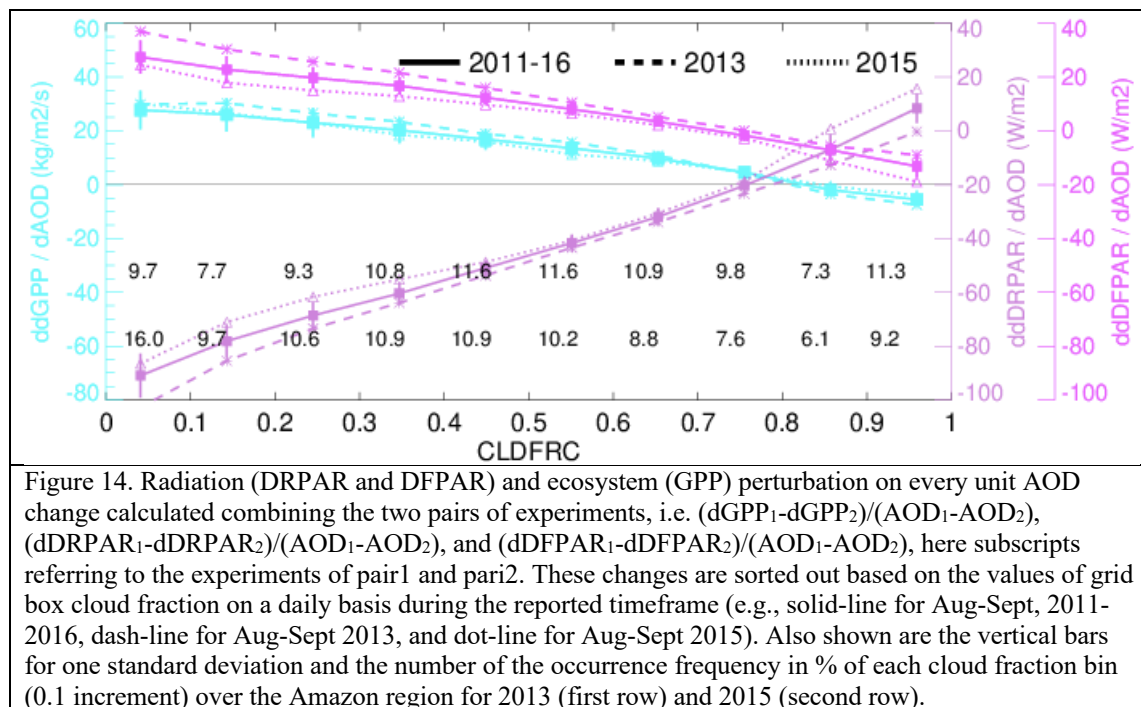752 of clouds in tempering the aerosol diffuse radiation fertilization effect.
753
754

Figure 14. Radiation (DRPAR and DFPAR) and ecosystem (GPP) perturbation on every unit AOD change calculated combining the two pairs of experiments, i.e. $(dGPP_1-dGPP_2)/(AOD_1-AOD_2)$, $(dDRPAR_1-dDRPAR_2)/(AOD_1-AOD_2)$, and $(dDFPAR_1-dDFPAR_2)/(AOD_1-AOD_2)$, here subscripts referring to the experiments of pair1 and pari2. These changes are sorted out based on the values of grid box cloud fraction on a daily basis during the reported timeframe (e.g., solid-line for Aug-Sept, 2011-2016, dash-line for Aug-Sept 2013, and dot-line for Aug-Sept 2015). Also shown are the vertical bars for one standard deviation and the number of the occurrence frequency in % of each cloud fraction bin (0.1 increment) over the Amazon region for 2013 (first row) and 2015 (second row).

755
756   **4. Conclusions**
757 We use the NASA GEOS ESM system with coupled aerosol, cloud, radiation, and ecosystem
758 modules to investigate the impact of biomass burning aerosols on plant productivity across the
759 Amazon Basin under the natural background cloud fields experienced during 2010-2016 – a
760 period containing a broad range of cloudiness conditions. We find that the biomass burning
761 aerosol DRFE does stimulate plant growth and has a notable impact on Amazon ecosystem
762 productivity during the biomass burning season (August-September). In the long-term mean, the
763 aerosol light fertilizer increases DFPAR by 3.8% and decreases DRPAR by 5.4%, allowing it to
764 increase Amazon GPP by 2.6%. On a monthly basis, the DRFE can increase GPP by up to 9.9%.
765 Consequently, biomass burning aerosols increase Amazonia yearly NPP by 1.5% on average,
766 with yearly increases ranging from 0.06% to 4.2% over the seven years studied. This 1.5% NPP
767 enhancement (or ~92TgC yr^{-1}) is equivalent to ~37% of the carbon loss due to Amazon fires.
768
769 The aerosol DRFE is strongly dependent on the presence of clouds, much stronger in clear sky
770 conditions and decreases with the increase of cloudiness. A fairly robust linear relationship is
771 found between cloud cover fraction and the sensitivity of radiation and GPP change to a change
772 in biomass burning AOD. BB aerosols stimulate plant growth under clear-sky conditions but
773 suppress it under full cloudiness conditions. Over the Amazon region within our study period,
774 the cloud fraction at which a unit AOD switches from stimulating to inhibiting plant growth
775 occurs at ~0.8. Note, however, that while our results show a clear sensitivity of the aerosol
776 DRFE to cloudiness, interannual variations in the aerosol light fertilizer's overall effectiveness
777 are controlled primarily by interannual variations in biomass burning aerosols during our studied

778   period because biomass burning AOD can vary by a factor of 6 from year to year. The associated
779   large variations in BBAOD are inevitably propagated to the radiation and ecosystem fields.
780   Overall, our work indicates that feedbacks between aerosols, radiation, and the ecosystem need
781   to be performed in the context of an atmospheric environment with a cloud presence.
782
783   This study examines the potential for the biomass burning aerosol DRFE to stimulate growth in
784   unburned forest over the Amazon basin. The net feedback of Amazon fires on the Amazon
785   biome is still an open question. Some changes, such as increasing atmospheric CO_2 and aerosols,
786   serve as forest fertilizers, whereas others, such as increasing O_3 pollution levels and the
787   deposition of smoke particles on plant leaves, reduce plant photosynthesis. On top of this, fires
788   also induce changes in meteorological fields (e.g., temperature, precipitation, clouds) that can
789   affect plant growth (Malavelle et al., 2019; Strada and Unger, 2016; Unger et al., 2017). More
790   efforts are needed to investigate the ecosystem effect of Amazon fires by integrating all these
791   potential factors.
792

807

808   **Data Availability:**
809   All of the observational data used in this study are publicly accessible, e.g., AERONET
810   (https://aeronet.gsfc.nasa.gov), CERES-EBAF (https://ceres.larc.nasa.gov/data/), FluxCom
811   (http://www.fluxcom.org), FluxSat (https://avdc.gsfc.nasa.gov), and GoAmazon
812   (https://www.arm.gov/research/campaigns/amf2014goamazon). The GEOS model results can be
813   provided by contacting with the corresponding author.
814

815   **Author contributions:**
816   H.B. took an overall responsible for the experiment design, model simulation, and data analysis.
817   E.L., R. D. K., S. P. M., and F. Z. contributed to the ecosystem study, D. O. B. contributed to the
818   cloud study, M. C., P. R. C., A. S. D, M. E. M., and H. Y. contributed to the aerosol study and
819   the model-observation comparison, P. N. contribute to the radiation study, and J. S. provided the
820   GoAmazon results. All authors contributed to the paper writing.
821

822

823   **References:**

Abdul-Razzak, H. and Ghan, S.: A parameterisation of aerosol activation 2. Multiple aerosol types, J. Geophys. Res., 105, 6837–6844, 2000.

Barahona, D. and Nenes, A.: Parameterizing the competition be- tween homogeneous and heterogeneous freezing in cirrus cloud formation – monodisperse ice nuclei, Atmos. Chem. Phys., 9, 369–381, doi:10.5194/acp-9-369-2009, 2009

Barahona, D., Molod, A., Bacmeister, J., Nenes, A., Gettelman, A., Morrison, H., Phillips, V., and Eichmann, A.: Development of two-moment cloud microphysics for liquid and ice within the NASA Goddard Earth Observing System Model (GEOS-5), Geoscientific Model 10 Development, 7, 1733–1766, 2014.

Bian, H., and M. J. Prather, Accurate simulation of stratospheric photolysis in global chemical model. J. Atmos. Chem., 41, 281-296, 2002.

Bian, H., M. Chin, S. R. Kawa, H. Yu, T. Diehl (2010), Multi-scale carbon monoxide and aerosol correlations from MOPITT and MODIS satellite measurements and GOCART model: implication for their emissions and atmospheric evolutions, J. Geophys. Res., 115, D07302, doi:10.1029/2009JD012781.

Bian, H., P. Colarco, M. Chin, G, Chen, J. M. Rodriguez, Q. Liang, D. Blake, D. A. Chu, A. da Silva, A. S. Darmenov, G. Diskin, H. E. Fuelberg, G. Huey, Y. Kondo, J. E. Nielsen, X. Pan, and A. Wisthaler (2013), Source attributions of pollution to the western Arctic during the NASA ARCTAS field campaign, Atmos. Chem. Phys., 13, 4707–4721.

Bian, H., M. Chin, D. A. Hauglustaine, M. Schulz, G. Myhre, S. E. Bauer, M. T. Lund, V. A. Karydis, T. L. Kucsera, X. Pan, A. Pozzer, R. B. Skeie, S. D. Steenrod, K. Sudo, K. Tsigaridis, A. P. Tsimpidi, and S. G. Tsyro (2017), Investigation of global particulate nitrate from the AeroCom phase III experiment Atmos. Chem. Phys., 17, 12911–12940 (https://www.atmos-chem-phys.net/17/12911/2017/).

Bian, H., Froyd, K., Murphy, D. M., Dibb, J., Darmenov, A., Chin, M., Colarco, P. R., da Silva, A., Kucsera, T. L., Schill, G., Yu, H., Bui, P., Dollner, M., Weinzierl, B., and Smirnov, A.: Observationally constrained analysis of sea salt aerosol in the marine atmosphere, Atmos. Chem. Phys., 19, 10773–10785, https://doi.org/10.5194/acp-19-10773-2019, 2019.

Breen, K. H., D. Barahona, T. Yuan, H. Bian, and S. C. James, Effect of volcanic emissions on clouds during the 2008 and 2018 Kilauea degassing events, https://doi.org/10.5194/acp-2020-979, 2020.

Butt, N., M. New, Y. Malhi, A. C. Lola da Costa, P. Oliveira, and J. E. Silva-Espejo (2010), Diffuse radiation and cloud fraction relationships in two contrasting Amazonian rainforest sites, Agric. For. Meteorol., 150(3), 361–368.

Carn, S., Fioletov, V., McLinden, C. *et al.* A decade of global volcanic SO_2 emissions measured from space. *Sci Rep* **7,** 44095 (2017). https://doi.org/10.1038/srep44095.

Chin, M., T. Diehl, O. Dubovik, T. F. Eck, B. N. Holben, A. Sinyuk, and D. G. Streets (2009), Light absorption by pollution, dust and biomass burning aerosols: A global model study and evaluation with AERONET data, Ann. Geophys., 27, 3439-3464.

Chin, M., Diehl, T., Tan, Q., Prospero, J. M., Kahn, R. A., Remer, L. A., Yu, H., Sayer, A. M., Bian, H., Geogdzhayev, I. V., Holben, B. N., Howell, S. G., Huebert, B. J., Hsu, N. C., Kim, D., Kucsera, T. L., Levy, R. C., Mishchenko, M. I., Pan, X., Quinn, P. K., Schuster, G. L., Streets, D. G., Strode, S. A., Torres, O., and Zhao, X.-P.: Multi-decadal aerosol variations from 1980 to 2009: a perspective from observations and a global model, Atmos. Chem. Phys., 14, 3657–3690, https://doi.org/10.5194/acp-14-3657-2014, 2014.

Chipperfield, M., Kinnison, D., Bekki, S., Bian, H., Brühl, C., Canty, T., et al. (2010). Stratospheric Chemistry (Chapter 6). In V. Eyring, T. G. Shepherd, & D. W. Waugh (Eds.), SPARC Report on the Evaluation of Chemistry-Climate Models. WCRP-132, WMO/TD No. 1526, SPARC Report No. 5 (pp. 191-252). Toronto: SPARC.

Colarco, P. R., A. da Silva, M. Chin, T. Diehl (2010), Online simulations of global aerosol distributions in the NASA GEOS-4 model and comparisons to satellite and ground-based aerosol optical depth, J. Geophys. Res., 115, D14207, doi:10.1029/2009JD012820.

Colarco, P. R., Gassó., S., Ahn, C., Buchard, V., Dasilva, A. M., & Torres, O. (2017). Simulation of the Ozone Monitoring Instrument aerosol index using the NASA Goddard Earth Observing System aerosol reanalysis products. Atmospheric Measurement Techniques. https://doi.org/10.5194/amt-10-4121-2017.

Cirino, G. G., R. A. F. Souza, D. K. Adams, and P. Artaxo, The effect of atmospheric aerosol particles and clouds on net ecosystem exchange in the Amazon, Atmos. Chem. Phys., 14, 6523–6543, 2014, www.atmos-chemphys.

Del Genio, A. D., M.-S. Yao, and J. Jonas (2007), Will moist convection be stronger in a warmer climate?, Geophys. Res. Lett., 34, L16703, doi:10.1029/2007GL030525.

Doughty, C. E., M. G. Flanner, and M. L. Goulden (2010), Effect of smoke on subcanopy shaded light, canopy temperature, and carbon dioxide uptake in an Amazon rainforest, Global Biogeochem. Cycles, 24, GB3015, doi:10.1029/2009GB003670.

Doughty, C.E., Metcalfe, D.B., Girardin, C.A.J., Farfan-Amezquita, F., Galiano Cabrera, D., Huaraca Huasco, W. et al. (2015). Drought impact on forest carbon dynamics and fluxes in Amazonia. Nature, 519:78–82.

Doughty, Russell, Philipp Köhler, Christian Frankenberg, Troy S. Magney, Xiangming Xiao, Yuanwei Qin, Xiaocui Wu, Berrien Moore. TROPOMI reveals dry-season increase of solar-induced chlorophyll fluorescence in the Amazon forest. Proceedings of the National Academy of Sciences, 2019; 201908157 DOI: 10.1073/pnas.1908157116.

Dubovik, O., Smirnov, A., Holben, B. N., King, M. D., Kauf- man, Y. J., Eck, T. F., and Slutsker, I.: Accuracy assessments of aerosol optical properties retrieved from AERONET Sun and sky-radiance measurements, J. Geophys. Res., 105, 9791–9806, 2000.

Dubovik, O., Holben, B. N., Eck, T. F., Smirnov, A., Kaufman, Y. J., King, M. D., Tanré, D., and Slutsker, I.: Variability of ab- sorption and optical properties of key aerosol types observed in worldwide locations, J. Atmos. Sci., 59, 590–608, 2002.

Edwards, J. M., and A. Slingo (1996), Studies with a flexible new radiation code. 1: Choosing a configuration for a large-scale model, W. J. R. Meteorol. Soc., 122(531), 689-719.

Ezhova, E., Ylivinkka, I., Kuusk, J., Komsaare, K., Vana, M., Krasnova, A., Noe, S., Arshinov, M., Belan, B., Park, S. B., Lavrič, J. V., Heimann, M., Petäjä, T., Vesala, T., Mammarella, I., Kolari, P., Bäck, J., Rannik, Ü., Kerminen, V. M., & Kulmala, M. (2018). Direct effect of aerosols on solar radiation and gross primary production in boreal and hemiboreal forests. *Atmospheric Chemistry and Physics*, **18**(24), 17,863– 17,881. https://doi.org/10.5194/acp-18-17863-2018.

Feldpausch, T. R., et al. (2016), Amazon forest response to repeated droughts, Global Biogeochem. Cycles, 30, 964–982, doi:10.1002/2015GB005133.

Feng, Y., Chen, D. & Zhao, X. Estimated long-term variability of direct and diffuse solar radiation in North China during 1959–2016. Theor Appl Climatol 137, 153–163 (2019). https://doi.org/10.1007/s00704-018-2579-1

Fountoukis, C. and Nenes, A.: Continued development of a cloud droplet formation parameterization for global climate models, J. Geophys. Res., 110, D11212, doi:10.1029/2004JD005591, 2005.

Gelaro, R., McCarty, W., Suárez, M. J., Todling, R., Molod, A., Takacs, L., et al. (2017). The Modern-Era Retrospective Analysis for Research and Applications, Version 2 (MERRA-2). Journal of Climate, 30(14), 5419–5454. https://doi.org/10.1175/JCLI-D-16-0758.1

Gu, L. H., D. D. Baldocchi, S. C. Wofsy, J. W. Munger, J. J. Michalsky, S. P. Urbanski, and T. A. Boden (2003), Response of a deciduous forest to the Mount Pinatubo eruption: Enhanced photosynthesis, Science, 299(5615), 2035–2038.

Guenther, A. B., X. Jiang, C. L. Heald, T. Sakulyanontvittaya, T. Duhl, L. K. Emmons and X. Wang (2012). "The Model of Emissions of Gases and Aerosols from Nature version 2.1 (MEGAN2.1): an

extended and updated framework for modeling biogenic emissions." Geosci. Model Dev. 5(6): 1471-1492.

Hall, S. R., Ullmann, K., Prather, M. J., Flynn, C. M., Murray, L. T., Fiore, A. M., Correa, G., Strode, S. A., Steenrod, S. D., Lamarque, J.-F., Guth, J., Josse, B., Flemming, J., Huijnen, V., Abraham, N. L., and Archibald, A. T.: Cloud impacts on photochemistry: building a climatology of photolysis rates from the Atmospheric Tomography mission, Atmos. Chem. Phys., 18, 16809–16828, https://doi.org/10.5194/acp-18-16809-2018, 2018.

Hemes, K. S., Verfaillie, J., and Baldocchi, D. D.: Wildfire-Smoke Aerosols Lead to Increased Light Use Efficiency Among Agricultural and Restored Wetland Land Uses in California's Central Valley, J. Geophys. Res.-Biogeo., 125, e2019JG005380, https://doi.org/10.1029/2019jg005380, 2020.

Hodzic A. and Jimenez J.L. (2011), Modeling anthropogenically controlled secondary organic aerosols in a megacity: a simplified framework for global and climate models. Geosci. Model. Dev., 4, 901-917, doi:10.5194/gmd-4-901-2011.

Huete, A. R., K. Didan, Y. E. Shimabukuro, P. Ratana, S. R. Saleska, L. R. Hutyra, W. Yang, R. R. Nemani, and R.

Myneni (2006), Amazon rainforests green-up with sunlight in dry season, Geophys. Res. Lett., 33, L06405, doi:10.1029/2005GL025583.

Iacono, M.J., J.S. Delamere, E.J. Mlawer, M.W. Shephard, S.A. Clough, and W.D. Collins, Radiative forcing by long-lived greenhouse gases: Calculations with the AER radiative transfer models, J. Geophys. Res., 113, D13103, doi:10.1029/2008JD009944, 2008.

Joiner, J., Yoshida, Y., Zhang, Y., Duveiller, G., Jung, M., Lya- pustin, A., Wang, Y., and Tucker, J. C.: Estimation of Terres- trial Global Gross Primary Production (GPP) with Satellite Data- Driven Models and Eddy Covariance Flux Data, Remote Sens., 10, 1346, https://doi.org/10.3390/rs10091346, 2018.

Jung, M., Schwalm, C., Migliavacca, M., Walther, S., Camps-Valls, G., Koirala, S., et al. (2020). Scaling carbon fluxes from eddy covariance sites to globe: synthesis and evaluation of the FLUXCOM approach. *Biogeosciences*, *17*(5), 1343–1365. https://doi.org/10.5194/bg-17-1343-2020

Kato, S., N. Loeb, F. G. Rose, D. R. Doelling, D. A. Rutan, T. E. Caldwell, L. Yu, and R. A. Weller (2013), Surface irradiances consistent with CERES-derived top-of-atmosphere shortwave and longwave irradiances. J. Climate, 26, 2719–2740, doi:10.1175/JCLI-D-12-00436.1.

Keppel-Aleks, G., and Washenfelder, R.A. 2016. "The effect of atmospheric sulfate reductions on diffuse radiation and photosynthesis in the United States during 1995–2013." Geophysical Research Letters, Vol. 43(No. 18): pp. 9984–9993. doi:10.1002/2016GL070052.

Kim, P. S., et al. (2015), Sources, seasonality, and trends of southeast US aerosol: an integrated analysis of surface, aircraft, and satellite observations with the GEOS-Chem chemical transport model, Atmos. Chem. Phys., 15, 10411-10433, doi:10.5194/acp-15-10411-2015.

Koster, R. D., M. J. Suarez, A. Ducharne, M. Stieglitz, and P. Kumar, 2000: A catchment-based approach to modeling land surface processes in a general circulation model: 1. Model structure. J. Geophys. Res., 105, 24 809–24 822, doi:10.1029/2000JD900327.

Koster, R. D., and G. K. Walker (2015), Interactive vegetation phenology, soil moisture, and monthly temperature forecasts, J. Hydrometeorol., 16, 1456–1465, doi:10.1175/JHM-D-14-0205.1.

Laurance, W.F. 1999. Gaia's lungs: Are rainforests inhaling Earth's excess carbon dioxide? Natural History (April), p. 96.

Lawrence, D. M., Fisher, R. A., Koven, C. D., Oleson, K. W., Swenson, S. C., Bonan, G., et al. (2019). The Community Land Model version 5: Description of new features, benchmarking, and impact of forcing uncertainty. Journal of Advances in Modeling Earth Systems, https://doi.org/10.1029/2018MS001583.

Min S. Lee, David Y. Hollinger, Trevor F. Keenan, Andrew P. Ouimette, Scott V. Ollinger, Andrew D. Richardson, Model-based analysis of the impact of diffuse radiation on CO2 exchange in a temperate

975   deciduous forest, Agricultural and Forest Meteorology, 249, 377-389,
976   https://doi.org/10.1016/j.agrformet.2017.11.016, 2018.
977 Letts, M. G., P.M. Lafleur, and N.T. Roulet, On the relationship between cloudiness and net ecosystem
978   carbon dioxide exchange in a peatland ecosystem Ecoscience, 12 (1) (2005), pp. 53–59.
979 Li, T. and Q. Yang, Advantages of diffuse light for horticultural production and perspectives for further
980   research. Front Plant Sci. 2015; 6: 704, published online 2015 Sep 4. doi: 10.3389/fpls.2015.00704.
981 Li, W., R. Fu, and R. E. Dickinson (2006), Rainfall and its seasonality over the Amazon in the 21st
982   century as assessed by the coupled models for the IPCC AR4, J. Geophys. Res., 111, D02111,
983   doi:10.1029/2005JD006355.
984 Malavelle, F. F., Haywood, J. M., Mercado, L. M., Folberth, G. A., Bellouin, N., Sitch, S., and Artaxo, P.:
985   Studying the impact of biomass burning aerosol radiative and climate effects on the Amazon
986   rainforest productivity with an Earth system model, Atmos. Chem. Phys., 19, 1301–1326,
987   https://doi.org/10.5194/acp-19-1301-2019, 2019.
988 Martin, S. T., Artaxo, P., Machado, L. A. T., Manzi, A. O., Souza, R. A. F., Schumacher, C., Wang, J.,
989   Andreae, M. O., Barbosa, H. M. J., Fan, J., Fisch, G., Goldstein, A. H., Guenther, A., Jimenez, J. L.,
990   Pöschl, U., Silva Dias, M. A., Smith, J. N., and Wendisch, M.: Introduction: Observations and
991   Modeling of the Green Ocean Amazon (GoAmazon2014/5), Atmos. Chem. Phys., 16, 4785–4797,
992   https://doi.org/10.5194/acp-16-4785-2016, 2016.
993 Mercado, L. M., N. Bellouin, S. Sitch, O. Boucher, C. Huntingford, M. Wild, and P. M. Cox (2009),
994   Impact of changes in diffuse radiation on the global land carbon sink, Nature, 458(7241), 1014–1017.
995 Molod, A., L. Takacs, M. Suarez, J. Bacmeister, I.-S. Song, and A. Eichmann, 2012. The GEOS-5
996   Atmospheric General Circulation Model: Mean Climate and Development from MERRA to Fortuna.
997   Technical Report Series on Global Modeling and Data Assimilation, 28, 2012
998   (http://gmao.gsfc.nasa.gov/ pubs/docs/Molod484.pdf).
999 Molod, A., Takacs, L., Suarez, M., and Bacmeister, J.: Development of the GEOS-5 atmospheric general
1000   circulation model: evolu- tion from MERRA to MERRA2, Geoscientific Model Development, 8,
1001   1339–1356, https://doi.org/10.5194/gmd-8-1339-2015, https: //www.geosci-model-
1002   dev.net/8/1339/2015/, 2015.
1003 Moreira, D. S., Longo, K. M., Freitas, S. R., Yamasoe, M. A., Mer- cado, L. M., Rosário, N. E., Gloor, E.,
1004   Viana, R. S. M., Miller, J. B., Gatti, L. V., Wiedemann, K. T., Domingues, L. K. G., and Correia, C.
1005   C. S.: Modeling the radiative effects of biomass burning aerosols on carbon fluxes in the Amazon
1006   region, Atmos. Chem. Phys., 17, 14785–14810, https://doi.org/10.5194/acp-17- 14785-2017, 2017.
1007 Murphy, D. M., Froyd, K. D., Bian, H., Brock, C. A., Dibb, J. E., DiGangi, J. P., Diskin, G., Dollner, M.,
1008   Kupc, A., Scheuer, E. M., Schill, G. P., Weinzierl, B., Williamson, C. J., and Yu, P.: The distribution
1009   of sea-salt aerosol in the global troposphere, Atmos. Chem. Phys., 19, 4093-4104,
1010   https://doi.org/10.5194/acp-19-4093-2019, Apr., 2019.
1011 Myneni, R., Knyazikhin, Y., Park, T. (2015). MOD15A2H MODIS Leaf Area Index/FPAR 8-Day L4
1012   Global 500m SIN Grid V006. NASA EOSDIS Land Processes DAAC.
1013   http://doi.org/10.5067/MODIS/MOD15A2H.006 (Terra) and
1014   http://doi.org/10.5067/MODIS/MYD15A2H.006 (Aqua).
1015 Napstad, D., C. M. Stickler, B. Soares-Filho, and F. Merry, Interactions among Amazon land use, forests
1016   and climate: prospects for a near-term forest tipping point**, Philos Trans R Soc Lond B Biol Sci.;
1017   363(1498): 1737–1746, doi: 10.1098/rstb.2007.0036, May 27, 2008.
1018 Nepstad DC, Stickler CM, Filho BS, Merry F. Interactions among Amazon land use, forests and climate:
1019   prospects for a near-term forest tipping point. Philos Trans R Soc Lond B Biol Sci.
1020   2008;363(1498):1737-1746. doi:10.1098/rstb.2007.0036.
1021 Ng, N. L., S. C. Herndon, A. Trimborn, M. R. Canagaratna, P. L. Croteau, T. B. Onasch, D. Sueper, D. R.
1022   Worsnop, Q. Zhang, Y. L. Sun and J. T. Jayne (2011). "An Aerosol Chemical Speciation Monitor
1023   (ACSM) for Routine Monitoring of the Composition and Mass Concentrations of Ambient Aerosol."
1024   Aerosol Science and Technology 45(7): 780-794.

1025 Niyogi, D., et al. (2004), Direct observations of the effects of aerosol loading on net ecosystem CO2
1026   exchanges over different landscapes, Geophys. Res. Lett., 31, L20506, doi:10.1029/2004GL020915.
1027 Oliveira, P. H. F., P. Artaxo, C. Pires, S. De Lucca, A. Procopio, B. Holben, J. Schafer, L. F. Cardoso, S.
1028   C. Wofsy, and H. R. Rocha (2007), The effects of biomass burning aerosols and clouds on the CO2
1029   flux in Amazonia, Tellus, Ser. B, 59(3), 338–349.
1030 Oleson, K. W., and Coauthors, 2010: Technical description of version 4.0 of the Community Land Model
1031   (CLM). NCAR Tech. Note NCAR/TN-478+STR, 257 pp.
1032 Oleson, K. W., Lawrence, D. M., Bonan, G. B., Drewniak, B., Huang, M., Koven, C. D., Levis, S., Li,
1033   F., Riley, W. J., Subin, Z. M., Swenson, S. C., Thornton, P. E., Bozbiyik, A., Fisher, R., Heald, C.
1034   L., Kluzek, E., Lamarque, J.-F., Lawrence, P. J., Leung, L. R., Lipscomb, W., Muszala, S., Ricciuto,
1035   D. M., Sacks, W., Sun, Y., Tang, J., & Yang, Z.-L. (2013). Technical description of version 4.5 of
1036   the Community Land Model (CLM), NCAR Tech. Note NCAR/TN-503+STR. National Center for
1037   Atmospheric Research, Boulder, Colorado, 420 pp.
1038 O'Sullivan, M., A. Rap, C. L. Reddington, D. V. Spracklen, M. Gloor, W. Buermann, Small global
1039   effect on terrestrial net primary production due to increased fossil fuel aerosol emissions
1040   from East Asia since the turn of the century, Geophys Res Lett. 2016 Aug 16; 43(15): 8060–
1041   8067. doi: 10.1002/2016GL068965, 2016.
1042 Rap, A., Spracklen, D. V., Mercado, L., Reddington, C. L., Haywood, J. M., Ellis, R. J., Phillips, O. L.,
1043   Artaxo, P., Bonal, D., Restrepo Coupe, N., and Butt, N.: Fires increase amazon forest productivity
1044   through increases in diffuse radiation, Geophys. Res. Lett., 42, 4654–4662
1045   doi:10.1002/2015GL063719, 2015.
1046 Rap, A., Scott, C.E., Reddington, C.L. et al. Enhanced global primary production by biogenic aerosol via
1047   diffuse radiation fertilization. Nature Geosci 11, 640–644 (2018). https://doi.org/10.1038/s41561-
1048   018-0208-3.
1049 Randles, C. A., Kinne, S., Myhre, G., Schulz, M., Stier, P., Fischer, J., Doppler, L., Highwood, E., Ryder,
1050   C., Harris, B., Huttunen, J., Ma, Y., Pinker, R. T., Mayer, B., Neubauer, D., Hitzenberger, R.,
1051   Oreopoulos, L., Lee, D., Pitari, G., Di Genova, G., Quaas, J., Rose, F. G., Kato, S., Rumbold, S. T.,
1052   Vardavas, I., Hatzianastassiou, N., Matsoukas, C., Yu, H., Zhang, F., Zhang, H., and Lu, P.:
1053   Intercomparison of shortwave radiative transfer schemes in global aerosol modeling: results from the
1054   AeroCom Radiative Transfer Experiment, Atmos. Chem. Phys., 13, 2347–2379,
1055   https://doi.org/10.5194/acp-13-2347-2013, 2013.
1056 Randles, C. A., da Silva, A. M., Buchard, V., Colarco, P. R., Darmenov, A., Govindaraju, R., et al.
1057   (2017). The MERRA-2 Aerosol Reanalysis, 1980 Onward. Part I: System Description and Data
1058   Assimilation Evaluation. Journal of Climate. https://doi.org/10.1175/JCLI-D-16-0609.1
1059 Rienecker, M. M., M. J. Suarez, R. Gelaro, R. Todling, J. Bacmeister, E. Liu, M. G. Bosilovich, S. D.
1060   Schubert, L. Takacs, G.-K. Kim, S. Bloom, J. Chen, D. Collins, A. Conaty, A. da Silva, W. Gu, J.
1061   Joiner, R. D. Koster, R. Lucchesi, A. Molod, T. Owens, S. Pawson, P. Pegion, C. R. Redder, R.
1062   Reichle, F. R. Robertson, A. G. Ruddick, M. Sienkiewicz, J. Woollen, MERRA - NASA's Modern-
1063   Era Retrospective Analysis for Research and Applications. J. Climate, 24, 3624–3648, 2011.
1064 Roderick, M. L., G. D. Farquhar, S. L. Berry, and I. R. Noble (2001), On the direct effect of clouds and
1065   atmospheric particles on the productivity and structure of vegetation, Oecologia, 129(1), 21–30.
1066 Saatchi S, Asefi-Najafabady S, Malhi Y, Arag~ao LEOC, Anderson LO, Myneni RB, Nemani R (2013)
1067   Persistent effects of a severe drought on Amazonian forest canopy. Proceedings of the National
1068   Academy of Sciences of the United States of America, 110, 565–570.
1069 Schmidt, G. A., et al. (2014), Configura-tion and assessment of the GISS Mod-elE2 contributions to the
1070   CMIP5 archive, J. Adv. Model. Earth Syst., 6, 141–184, doi:10.1002/2013MS000265.
1071 Shilling, J. E., M. S. Pekour, E. C. Fortner, P. Artaxo, S. de Sá, J. M. Hubbe, K. M. Longo, L. A. T.
1072   Machado, S. T. Martin, S. R. Springston, J. Tomlinson and J. Wang (2018). "Aircraft Observations of
1073   Aerosol in the Manaus Urban Plume and Surrounding Tropical Forest during GoAmazon 2014/15."
1074   Atmos. Chem. Phys. Discuss. 2018: 1-37.

1075 Sporre, M. K., Blichner, S. M., Karset, I. H. H., Makkonen, R., and Berntsen, T. K.: BVOC–aerosol–
1076   climate feedbacks investigated using NorESM, Atmos. Chem. Phys., 19, 4763–
1077   4782, https://doi.org/10.5194/acp-19-4763-2019, 2019.
1078 Strada, S. and Unger, N.: Potential sensitivity of photosynthesis and isoprene emission to direct radiative
1079   effects of atmospheric aerosol pollution, Atmos. Chem. Phys., 16, 4213–4234,
1080   https://doi.org/10.5194/acp-16-4213-2016, 2016.
1081 Thornton, P. E., & Zimmermann, N. E. (2007). An improved canopy integration scheme for a land
1082   surface model with prognostic canopy structure. Journal Of Climate, 20, 3902-3923.
1083   doi:10.1175/JCLI4222.1.
1084 Unger, N., Yue, X., and Harper, K. L.: Aerosol climate change effects on land ecosystem services,
1085   Faraday Discuss., 200, 121–142, https://doi.org/10.1039/c7fd00033b, 2017.
1086 University of Oklahoma. "Dry season increase in photosynthesis in Amazon rain forest." ScienceDaily.
1087   ScienceDaily, 22 October 2019. <www.sciencedaily.com/releases/2019/10/191022092804.htm>
1088 Wang, X., Wu, J., Chen, M., Xu, X., Wang, Z., Wang, B., Wang, C., Piao, S., Lin, W., & Miao,
1089   G. (2018). Field evidences for the positive effects of aerosols on tree growth. *Global Change*
1090   *Biology*, **24**, 4983– 4992. https://doi.org/10.1111/gcb.14339.
1091 Wild, O., X. Zhu, and M. Prather, Fast-J: Accurate simulation of in- and below-cloud photolysis in
1092   tropospheric chemical models, J. Atmos. Chem. 37, 245-282, 2000.
1093 Xi, X., and I. N. Sokolik, 2012: Impact of Asian dust aerosol and surface albedo on photosynthetically
1094   active radiation and surface radiative balance in dryland ecosystems. Advances in Meteorology, 2012,
1095   Article ID 276207, doi: 10.1155/2012/276207.
1096 Yan, X., W. Z. Shi, W. J. Zhao, et al., 2014: Impact of aerosols and atmospheric particles on plant leaf
1097   proteins. Atmos. Environ., 88, 115–122, doi: https://doi.org/10.1016/j.atmosenv.2014.01.044.
1098 Zhou, Yanlian; Xiaocui Wu; Weimin Ju; Leiming Zhang; Zhi Chen; Wei He; Yibo Liu; Yang Shen,
1099   Modeling the Effects of Global and Diffuse Radiation on Terrestrial Gross Primary Productivity in
1100   China Based on a Two-Leaf Light Use Efficiency Model, *Remote Sens. 12*(20),
1101   3355; https://doi.org/10.3390/rs12203355, 2020.